21 May 2003

The SNAP Wide Area Survey

James Annis, Fritz DeJongh, Josh Frieman, Lam Hui, Huan Lin, John Marriner, Vic Scarpine, Albert Stebbins, Chris Stoughton, William Wester, Steve Kent[1], Peter Limon[1],

ABSTRACT

The SuperNova Acceleration Probe (SNAP) is a mission proposed to probe Dark Energy using observations of high-redshift supernovae, but it is also uniquely positioned to implement other, complementary probes of Dark Energy. These probes include weak lensing cosmic shear and the evolution of the abundance of galaxy clusters. These probes offer the promise of determining the Dark Energy equation of state with a precision comparable to that of the supernovae, while subject to completely independent systematic errors. Understanding the nature of the Dark Energy is critical for progress in fundamental physics and therefore demands that we bring to bear multiple techniques.

While the SNAP supernova survey is deep and narrow (15 square degrees), weak lensing and cluster counting require wider sky coverage in order to usefully probe the Dark Energy. As a result, the SNAP collaboration is considering a shallower, but broader (300 square degree) wide area survey in addition to the supernova survey.

In this White Paper, we report on an on-going study by the Fermilab SNAP group aimed at optimizing the design of the SNAP wide area survey as a Dark Energy machine. We overview the weak lensing and cluster abundance methods and show their sensitivities to Dark Energy as a function of survey area and depth within the parameters set by the mission hardware. We also touch on other collateral science benefits of the wide area survey, such as the evolution of large-scale structure.

Our preliminary studies indicate that increasing the sky coverage of the SNAP wide area survey to 1000 square degrees can yield critical improvements in its Dark Energy reach. This may entail a need for larger data rate and overall data volume than currently envisioned for the mission. We describe a program of hardware related research being undertaken at Fermilab, aimed in part at achieving the wide area survey. This includes focal plane electronics, data compression, on-board storage, and data transmission. Along with the radiation shield, these are areas in which Fermilab expects to play a major role in the project.

The wide area survey also has special software requirements in addition to those for the supernova survey. Building on the expertise developed through experience in the Sloan Digital Sky Survey (SDSS), this is also an area where Fermilab plans to take

[1]SNAP Fermilab PIs

on a leadership role, developing a pipeline for processing, co-adding, and analyzing the imaging data and technologies for a data factory and distribution.

The Fermilab group is driven by the scientific goal of uncovering the nature of the Dark Energy, both via supernovae and the other methods, and is particularly interested in the prospects for the SNAP wide area survey. In addition to the technical hardware and software expertise we will bring to SNAP, Fermilab has the human talent and experience in place to play a major scientific leadership role in the wide area survey (regardless of its sky coverage). For example, Fermilab scientists have been active in using the SDSS to measure weak lensing, the cluster abundance, and large-scale structure. We describe plans to develop simulations and data analysis tools to refine the wide area optimization study and eventually carry out these analyses on real data.

1. Introduction

The particle physics/cosmology frontier– In 1983, the Theoretical Astrophysics Group was established at Fermilab to explore the fertile connections between high-energy physics and the early Universe. In the intervening twenty years, these connections have deepened and have begun yielding to experimental tests. In 1991 the Experimental Astrophysics Group was established to work on the Sloan Digital Sky Survey (SDSS), its aim to measure the large scale structure of the Universe and thereby probe the dark matter. The SDSS has been a spectacularly successful project, yielding new insights into large-scale structure, the most distant quasars, the thermal history of the Universe, and the structure of our own galaxy. More recently, Fermilab joined the Cold Dark Matter Search (CDMS) experiment to directly detect particle dark matter, a signature of supersymmetry, from the Milky Way. The Lab is also involved in the Pierre Auger Observatory to measure the highest energy cosmic rays (UHECR). Now, Fermilab is positioned to pursue the most remarkable discovery of the particle physics/cosmology frontier: the bulk of the energy density in the Universe is in an unknown, exotic form, known as Dark Energy. A key element linking these phenomena—dark matter, UHECR, and dark energy—is that they almost certainly point to physics beyond the Standard Model.

Dark energy– In 1998, two independent groups (The High-z Supernova Search, Garnavich et al. (1998); Riess et al. (1998); Schmidt et al. (1998), and the Supernova Cosmology Project, Perlmutter et al. (1999)) measured the brightnesses of distant supernovae and found evidence that the expansion of the Universe is accelerating rather than decelerating. This discovery implies that the energy density of the Universe is dominated by an unknown, negative pressure component, now called Dark Energy, characterized by an equation of state, $w = p/\rho$, with $w < -1/3$. Confirming, but indirect, evidence for dark energy comes from measurements of the cosmic microwave background anisotropy, which point to $\Omega_{tot} = 1$ (where Ω is the density of some mass component relative to the critical density for a flat Universe), and large-scale galaxy surveys which indicate

$\Omega_m = 0.3$ in "ordinary" (mostly dark) matter. There must be a 'missing energy' component with $\Omega = 0.7$; in order for galaxies to have formed, the missing energy must have come to dominate at very late times, implying $w < -1/2$ (see Carroll (2001); Peebles and Ratra (2003) for reviews). It is also possible that the Dark Energy signifies not a new energy component but a modification of Einstein's General Relativity at large distances—in either case, the consequences for fundamental physics are profound.

A cosmological constant—traditionally interpreted as the energy associated with the vacuum—is the simplest possibility for dark energy: in this case, the vacuum energy scale is of order 10^{-3} eV and the dark energy equation of state $w = -1$. However, particle physics theory, including string theory, indicates that the energy scale of the vacuum should be at least of order the super-symmetry breaking scale, fifteen orders of magnitude higher. In the absence of an explanation for this discrepancy—known as the Cosmological Constant problem—some have speculated that a new symmetry or dynamics may suppress the true vacuum energy scale or set it to zero. In this case, the dark energy may be a sign that the Universe is not yet in its ground state, and it could have an interesting dynamics. In such dynamical dark energy models (Frieman et al 1995) (also called 'quintessence' models), the equation of state parameter w may differ from -1 and is generically expected to evolve with time.

In this situation, it is clear that progress in understanding the nature of the Dark Energy requires more precise experimental determination of its equation of state. Fortunately, there are excellent prospects for developing and maturing complementary cosmological probes of the dark energy over the next decade. They include (a) deeper, larger supernova surveys with much improved control of systematic errors, (b) high-precision measurement of weak lensing cosmic shear, and (c) measurement of the evolution of the abundance of galaxy clusters. These probes have three successive aims: (i) to provide direct evidence for acceleration, to confirm the current supernovae results, (ii) to determine the equation of state w with sufficient precision that the cosmological constant ($w = -1$) can be reliably distinguished from the current upper bound of $w = -0.8$, and (iii) to measure the time evolution of w.

SNAP– SNAP is a proposed satellite equipped with a 2-meter telescope, wide-field optical and near infrared imaging cameras, and an integral-field spectrograph, designed to measure lightcurves and spectra for ~ 2000 supernovae out to redshifts $z = 1.7$. While SNAP is primarily designed to exploit the full potential of supernovae as precision probes of the dark energy, the hardware requirements of the supernova search also make it ideally suited to address the dark energy through the complementary methods of weak lensing and cluster counts. These alternative methods are experimentally less mature than the supernovae as dark energy probes but are being increasingly recognized by cosmologists as extremely promising. A preliminary design of a SNAP wide field survey covering 300 square degrees, in addition to the SNAP deep supernova survey of 16 square degrees, was aimed in particular at measuring cosmic shear and thereby constraining w. This prospect raises questions which this document attempts to address in part: (i) Is SNAP the right mission to implement the cosmic shear and cluster abundance probes? In particular, do these measurements require a space mission? (ii) If so, how should one design the SNAP wide field survey to yield maximum return in terms of dark energy constraints? (iii) How can Fermilab contribute technically and scientifically to the SNAP mission to make it a success? Is it well matched to our strengths and interests?

Measuring dark energy– Fundamentally, the dark energy impacts cosmological observables by affecting the Hubble expansion rate as a function of time. The expansion rate history determines the distance to an object as a function of its redshift and also the growth rate of density perturbations as a function of time. While supernovae probe the distance-redshift relation, cosmic shear and the cluster abundance are in principle sensitive to both the distance measure (through the volume element as a function of redshift) and the perturbation growth rate. In particular, for a spatially flat Universe (with $\Omega_{tot} = 1$), the Hubble expansion rate is given by

$$\frac{H^2(z)}{H_0^2} = \Omega_m(1+z)^3 + \Omega_{DE}(1+z)^{3(1+w)}\,, \tag{1}$$

where $H_0 = 72\pm8$ km/sec/Mpc, Ω_m is the present density of "ordinary" matter, Ω_{DE} is the present density of dark energy, and w is the dark energy equation of state (for illustration, here assumed to be constant but in general time dependent). The factors $(1+z)^n$ reflect how the densities of the matter and dark energy components scale with the volume of space; e.g., for a cosmological constant with $w = -1$, the vacuum energy density is time-independent. More generally, the dark energy density scales more slowly with volume than the matter density.

Supernovae provide a direct way to map the expansion history $H(z)$. Their attractiveness lies in their simplicity: type Ia supernovae are nearly standard candles—they have nearly identical peak luminosities—enabling one to measure the luminosity distance,

$$d_L(z) = (1+z)r(z)\,, \tag{2}$$

where $r(z)$ is the comoving distance to redshift z,

$$r(z) = \int_0^z \frac{dx}{H(x)}\,. \tag{3}$$

Weak lensing and cluster counting depend on the expansion history in different ways. In addition to the luminosity distance, the expansion history determines: the angular diameter distance,

$$d_A(z) = (1+z)^{-1}r(z)\,, \tag{4}$$

the comoving volume element at redshift z,

$$f(z) \equiv \frac{dV}{dzd\Omega} = r^2(z)/H(z)\,, \tag{5}$$

where Ω here is solid angle on the sky, and the rate at which cosmological density perturbations grow on large scales,

$$D(z) = \frac{5\Omega_m}{2} H(z) \int_0^z \frac{(1+z)}{H^3(z)} dz\,. \qquad (6)$$

Weak lensing is sensitive to the angular diameter distance (roughly, it probes the angle subtended by features in the matter power spectrum, which correspond to fixed comoving lengths) and to the density perturbation growth rate. Cluster counting experiments probe the volume element as well as the perturbation growth function.

Figure 1, from Huterer & Turner (2001), shows the sensitivity of these measures to the dark energy equation of state parameter w. At small redshifts $r(z)$ is insensitive to w for the simple reason that *all* cosmological models reduce to the Hubble law ($r = H_0^{-1}z$) for $z \ll 1$. At $z > 2$, there is little sensitivity to w because the dark energy density becomes subdominant compared to ordinary matter at high redshift. The sensitivities of $r(z)$ and $f(z)$ peak at redshifts around unity.

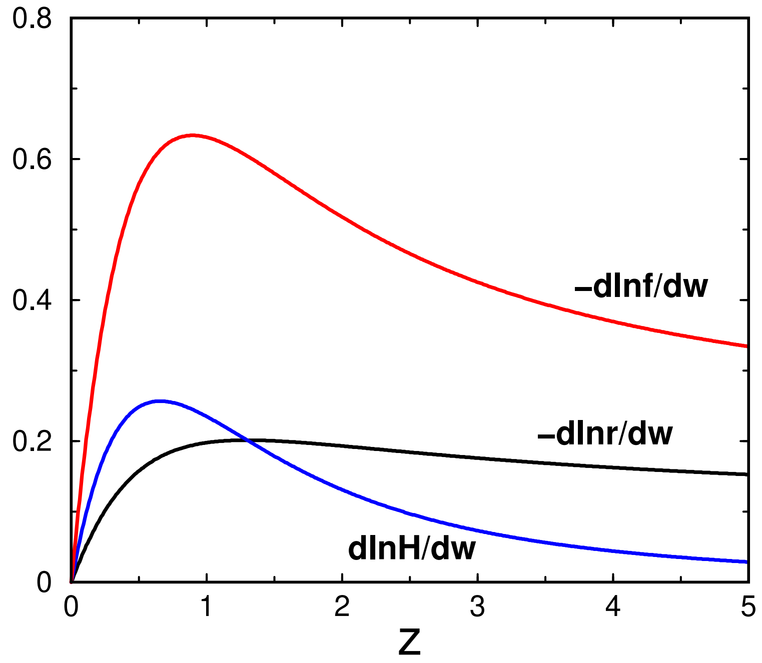

Fig. 1.— The relative sensitivity of $r(z)$, $f(z)$, and $H(z)$ to a change in the constant value of w.

Science outline– In this document, we lay out the design considerations and science case for the SNAP wide area survey, showing how trade-offs in survey area vs. depth impact the dark energy constraints that can be achieved via weak lensing and cluster counts. Our aim is a wide survey which provides dark energy probes of comparable or greater precision to the supernovae. The following sections cover:

- Wide Area Survey Design
- Cluster Abundance: Optical/IR Cluster Counts and the Growth Function
- Weak Lensing
- Non-Dark Energy Science

Subsequent sections describe the technical contributions Fermilab expects to make to the SNAP mission.

2. Wide Area Survey Design

2.1. Dark Energy Experiments: Supernovae, Cosmic Shear, and Clusters

Table 1 lists three complementary techniques that have been proposed for measuring dark energy along with current or future facilities that might carry out the observations within the next 10 years. In this chapter we compare the merits of each technique and the strengths and weaknesses of proposed experiments for making the necessary observations. The SNAP collaboration has made an extensive and compelling case for supernovae (Perlmutter 2002a) and for the necessity of a space-based supernova project to determine the dark energy equation of state w to $\sim 5\%$ accuracy. Our emphasis here is on the two other probes: (i) weak lensing cosmic shear and (ii) the abundance of galaxy clusters as a function of mass and redshift. These methods are independent of the supernovae, subject to completely different systematic errors, and can thus provide important cross-checks on the supernova results. In addition, these methods provide constraints in the Ω_m-w plane that are nearly orthogonal to the supernovae constraints; as a result, combining them with the supernova measurements helps break cosmological parameter degeneracies and leads to more precise parameter determinations than either can achieve on its own (See figure 2.).

Cosmic shear and cluster counting can in principle yield dark energy constraints comparable to or stronger than that achievable with supernovae. On the other hand, both of these methods rely on the cold dark matter paradigm for large-scale structure formation and are therefore sensitive to a larger number of cosmological parameters (e.g., the scale-dependence of the initial matter power spectrum, the neutrino mass, etc) as well as an understanding of gravitational instability in the non-linear regime. Despite the continuing challenge of modeling all the details of galaxy formation in depth, this structure formation paradigm has been tested in a number of ways and appears robust enough to be used as a tool for probing cosmology. Moreover, independent experiments, particularly measurements of the cosmic microwave background anisotropy from WMAP and Planck, will substantially reduce the uncertainties in these other cosmological parameters and therefore reduce the marginal uncertainties in the weak lensing and cluster probes of dark energy.

Supernovae– Supernovae provided the first direct evidence for dark energy, and the proposed SNAP mission is nearly optimal for exploiting the full potential of SNe Ia as precision probes of the dark energy. It will do this by achieving unprecedented control of the sources of systematic error and by amassing a large sample of SNe at redshifts $0.5 < z < 1.7$, where the dark energy leverage is largest (see Fig. 1). The goal of detecting and following up 2000 supernovae over this redshift range largely determines the survey area of 16 square degrees, the 2-meter telescope aperture, the number of optical and infrared filters needed, and the field of view of the imaging camera, shown in Fig. 3. Before SNAP flies, a number of large ground-based supernova surveys, many of them begun in recent months, will achieve improvements over the current w constraints by measuring light-curves for hundreds of SNe Ia at redshifts $z < 0.8$ over the next five years. In addition, the ACS/Goods survey with the Hubble Space Telescope (HST) will enlarge the sample of supernovae at redshifts

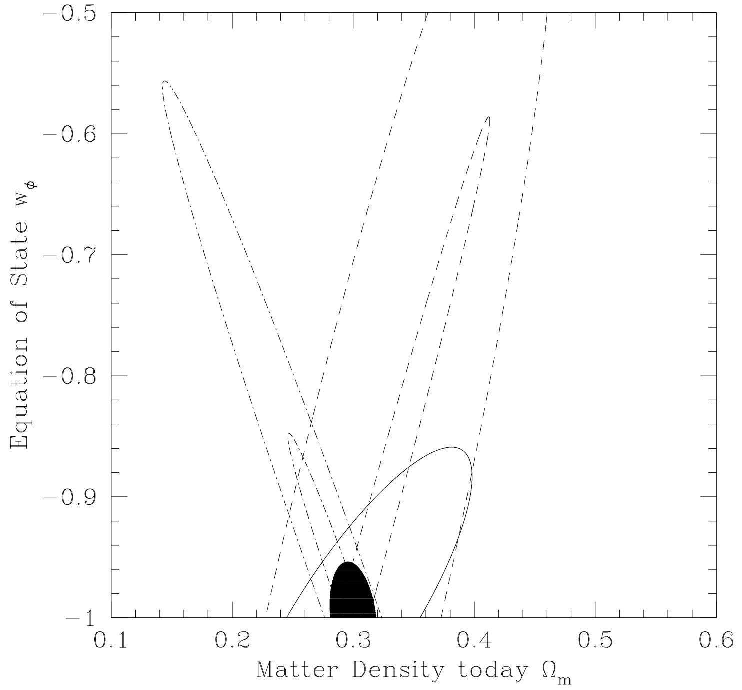

Fig. 2.— A plot (taken from Levine et al. (2002)) showing the idealized CMB constraints from WMAP and Planck (the inner and outer dashed lines, respectively), idealized SN constraints using 200 and 400 supernovae from a ground and space based experiment (outer and inner dot-dashed lines, respectively), and idealized constraints from a 1000 sq-degree x-ray based cluster counting experiment reaching $z = 1.2$ (the solid line). The solid region shows what one can do by performing joint constraints.

$z > 1$. There are, furthermore, initiatives to dedicate some fraction of the Hubble Space Telescope observing time to a supernova program [2] which if carried out could be quite powerful. However, the limitation to relatively 'low' redshifts from the ground, to optical (as opposed to near infrared (NIR)) observing, and the practical limits on photometric accuracy achievable from ground-based observatories (and HST) will leave room for substantial improvement in the determination of w and especially its time dependence $\dot{w}$. There is now broad consensus that a space-based observatory with long-term stability and NIR capability is necessary to reliably probe the $z > 1$ regime and therefore precisely constrain the dark energy (Kim 2002; Perlmutter 2002b).

Cluster counting– To probe the dark energy, both cluster counting and weak lensing require a different combination of depth of exposure and area on the sky—and thus a different survey—from the supernovae. For fixed survey depth, the precision on w for these methods scales approximately as $\sqrt{f_{sky}}$, where f_{sky} is the fraction of sky covered in the survey. The cosmological precision therefore scales as the square root of the total survey duration. If instead one fixes the survey area, the precision on dark energy increases relatively slowly with survey depth (limiting magnitude) and therefore scales more slowly than $\sqrt{t}$. As a result, for fixed survey duration, going wide is in general more efficient than going deep in order to probe cosmological parameters. This is obviously a gross oversimplification—other mitigating factors such as systematic errors generally lead to a floor on the survey depth below which these scaling arguments break down, and the incremental gains in dark energy precision for very wide area surveys (say, with $f_{sky} > 0.1$) are small (Levine et al. 2002). For example, although the SDSS will cover roughly 20% of the sky, it does not reach sufficient depth to implement the cluster and weak lensing probes of dark energy.

Cluster counting may be done in x-ray, optical, and submillimeter bandpasses. The x-ray and submillimeter techniques rely on the presence of $T \sim 10^8$ K gas in the gravitational potential wells of clusters. This gas emits x-rays via thermal bremsstrahlung; in the submillimeter, the Sunyaev-Zeldovich (SZ) effect—the Compton upscattering of CMB photons by the hot intracluster electrons—is detectable as a deficit in the CMB intensity at low frequencies. There are on-going efforts to pursue dark energy probes using both techniques. The DUET X-ray satellite mission has been (unsuccessfully) proposed to NASA in the past and will likely be revived in the future. Using the SZ effect, a number of groups are carrying out pilot cluster surveys over small areas of sky. In the next several years, these will be augmented by larger dedicated facilities (e.g., SZA and APEX); toward the end of this decade, a wide area ($\sim$ 4000 square degrees) SZ survey will be carried out with the 8-meter South Pole Telescope and possibly with the ACT in Chile. In order to be useful as dark energy probes, the SZ and X-ray cluster surveys will require extensive optical counterpart surveys to measure the redshifts of the clusters. Either the proposed Large Synoptic Survey Telescope (LSST), if sited in Chile, or a visible camera for ESO's 4-meter VISTA telescope

---

[2] See, for example, Space Telescope Science Institutes' report on the Scientific Case for an Extended HST Mission: http://www.stsci.edu/resources/sm5revise.pdf

(under construction) could provide the necessary optical, multi-band data for photometric redshifts. LSST would be a 6-8 meter telescope with a large optical camera covering a very wide field of view, very efficient for rapid sky surveys covering large fractions of the sky. [3]

Either LSST or VISTA could also be used in a cluster counting experiment pursued using optical cluster detection techniques, as described below for SNAP. They could also measure the cosmic shear weak lensing signal at moderate depth.

Table 1 shows the three main classes of dark energy probes and the experiments that aim to make the measurements. It is worth noting that only SNAP will be able to make measurements in all three classes.

Weak lensing– The LSST in particular is partially aimed at a 1000 square degree deep survey to use weak lensing to measure the matter power spectrum. Other programs such as the recently begun CFHT Legacy Survey aim at smaller sky areas but will be done before the end of the decade. LSST, at the end of a 10 year program, will also have a shallower $f_{sky} = 0.33$ survey that could be used in an optical cluster counting experiment.

2.2. Ground-based vs. Space-based Wide Field Surveys

As noted above, it has been shown that a space-based mission is critical for obtaining reliable measurements of high-redshift ($z > 1$) supernovae and thereby probing the dark energy. It is clear that a wide field survey from space is also *useful* for studying the dark energy via weak lensing and cluster counts, but is it *necessary*? This issue has been summarized in recent papers by Rhodes et al. (2003) and Massey et al. (2003b) and in more technical detail by Bernstein (2002).

Weak lensing from space– The weak lensing cosmic shear signal, which requires precise measurement of the shapes of millions of faint galaxies, is intrinsically small (typically of order 1% rms shear) and notoriously difficult. The ground-based measurements of cosmic shear carried out to date all show evidence of residual systematic errors (after correcting for much larger systematic errors, typically of order 10% rms 'shear', in the raw data) at a level comparable to the measured signal. A number of systematic effects can induce an apparent shearing or smearing of galaxy images: differential atmospheric refraction, wind shaking the telescope, temperature changes in the instrument and telescope optics, inaccurate telescope guiding, etc. To correct for these effects, one must measure the shapes and apparent sizes of stars (the point spread function or PSF) in the same area of sky. Since stellar images are subject to the same systematic effects, one can in a sense transform the images to make the stars round and thus correct the systematic effects on the galaxy

[3] Assuming it is funded, the first light for LSST is currently scheduled for 2012. The first light for the VISTA telescope is scheduled for 2006, although funding is not yet in hand for an optical camera.

images. Since the density of stars on the sky is finite, and the instrumental smearing is time- and position-dependent due to constantly changing atmospheric, thermal, and mechanical conditions, there is a limit to how well this 'PSF correction' procedure can work from the ground. In addition, the overall blurring of images due to atmospheric turbulence (called 'seeing') limits the resolution and makes it problematic to accurately measure and correct the shapes of small, faint galaxies.

As a result, weak lensing measurements put a premium on having high spatial resolution and a stable environment for the telescope and instruments. Both of these requirements argue for space-based observations: (i) without the blurring effect of the atmosphere, space-based resolution is set by the telescope size and pixel dimensions; SNAP will have 0.15 arcsecond resolution[4], compared to 0.5 arcsec seeing at the best ground-based sites, so it will be able to measure shapes for a larger fraction of faint galaxies; (ii) SNAP's orbit is designed to provide a very stable thermal environment, which means the PSF should be much more stable than can be achieved from the ground—this will substantially reduce systematic errors associated with the time-varying smearing of stars seen from the ground. Detailed studies by Rhodes et al. (2003) of the SNAP PSF, based on mechanical design of the telescope, indicate that it should be sufficiently stable so that residual systematics in the shear measurements will be under control.

Cluster counting from space– To measure the cluster abundance, one needs to reliably detect faint galaxies and determine their redshifts photometrically, using multi-band colors, to high redshift. This requires deep near-infrared (in addition to optical) imaging which cannot be done efficiently from the ground due to atmospheric absorption (over most IR wavelengths) and night sky airglow (in the IR windows; space has a factor of 10 lower background). Ground-based cluster surveys are therefore confined to lower redshifts, $z < 1.2$, and therefore have less leverage in constraining w and especially its time dependence. On the other hand, with its optical and NIR filters, SNAP can reach $z = 2.4$, and thus will have significantly higher sensitivity to the dark energy.

Note that the advantages of space for both cosmic shear and cluster counting depend to a significant degree on the depth of the survey. For shallow surveys, corresponding roughly to $R < 25$ and wavelengths bluer than 800 nm (Bernstein 2002), large ground-based telescopes such as the LSST can be more efficient at covering large areas of sky, provided the varying PSF residuals can be brought under better control than they are at present facilities. In this regime, a large fraction of the source galaxies can be resolved in conditions attainable at the best ground-based sites, and the larger source galaxy sizes imply less sensitivity to the PSF. In addition, the lower median redshift of a shallower survey means that a higher fraction of galaxy photometric redshifts can be determined without IR imaging. However, shallower surveys have less sensitivity to $\dot{w}$. have less sensitivity to $\dot{w}$.

[4]limited by CCD detector performance, not optics.

In sum, the substantial advantages of a space-based observatory for supernova measurements—better angular resolution, more stable environment, near IR capability, resulting in better sensitivity to time evolution of w—carry over to the cosmic shear and cluster abundance probes as well.

2.3. Wide Field Survey Design Parameters

Given the desirability of carrying out these measurements from space, how does one design a SNAP wide field survey to gain maximum dark energy leverage from cosmic shear and cluster counts? Given the telescope and focal plane specifications laid out by the SNAP collaboration, and given a fixed total amount of observing time for the wide survey, this issue comes down mainly to studying trade-offs in survey area vs. depth; a secondary variable is the number of optical filters needed to carry out these projects, along with their wavelength ranges.

In a series of three recent papers, the SNAP team has studied this issue with regard to cosmic shear. They assumed a total allotment of five months for the wide area survey and an individual frame exposure time of 500 sec set by current specified design limitations of the on-board data storage and of the satellite telemetry. These exposures are repeated 4 times in order to reject cosmic ray contamination, for a total exposure time of 2000 sec in each optical filter and 4000 sec in each NIR filter. This leads to a 300 square degree survey in all 9 SNAP filters (6 optical and 3 NIR). Below, we lay out a number of survey options, including this current default option, in order to see how the trade-offs in depth, area, and the number of filters used impact on the dark energy reach of the shear and cluster probes. In particular, several of the options relax one or more of the above assumptions: (i) we consider surveys of both 5- and 10-month durations, (ii) we assume that modest data compression beyond that currently specified in the mission design can enable storage of shorter (and therefore more) exposures if necessary (in order to survey larger total area), and (iii) in some cases, we consider the possibility of only using 3 of the 6 optical filters on any given point, which again allows larger area coverage in fixed survey time.

The eight survey options shown in Table 2 span a range of depths and survey areas—covering survey areas from 300 to 2000 square degrees, with the larger areas generally having shorter exposure times and consequently less depth. The motivation for this study was to see what gains in dark energy constraints could be made by going to larger survey area at a cost of modest depth reduction. The philosophy was to design a wide field survey that could yield dark energy constraints comparable to or more stringent than the SNAP supernovae, while still remaining in the depth regime ($R > 25$) that exploits the advantages of space. That philosophy led us to also consider the 10-month survey option: if that is what is needed to make these probes truly complementary in strength to the supernovae, it should be considered. Generally, one is led to sacrifice depth in favor of area: the statistical errors on the cosmic shear power spectrum and on the cluster abundance both scale roughly as the inverse square root of the survey area. While increasing area implies less depth, as noted above the scaling of the errors with survey limiting depth is less strong.

Table 1. Dark Energy Techniques and Experiments

Supernovae	Galaxy Clusters	Weak Lensing
(Direct, self-contained)	(Indirect, must combine with other experiments)	(Indirect, must combine with other experiments)
SNAP (Space)	SNAP (Space)	SNAP (Space)
HST/Keck (Space/Ground)	LSST (Ground)	LSST (Ground)
CFHT/CTIO/Magellan/... (Ground)	DUET (X-rays) (Space)	
	SPT (Sunyaev-Zel'dovich) (Ground)	

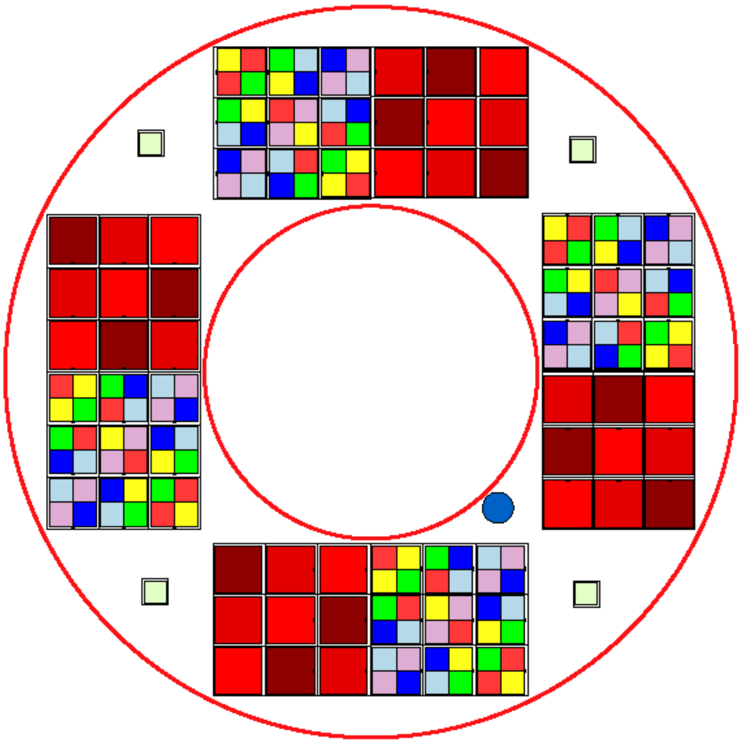

Fig. 3.— SNAP focal plane, showing the layout of the optical and infrared arrays. There are 4 identical detector mosaics. Each mosaic contains 9 optical CCDs and 9 NIR imagers. Each optical CCD is covered by a 2×2 grid of filters. Each infrared array is covered by a single filter.

Table 2. Wide Field Survey Parameters

Name	Area	Survey Time	Exp. Time	Flux Limit (I_{AB})	N_{source}
I (Default)	300	5	2000	26.5	100
II	300	10	4000	26.9	150
III	600	5	960	26.1	60
IV	600	10	2000	26.5	100
V (Fiducial)	1000	10	1170	26.2	70
VI	600 (1/2)	5	2000	26.5	100
VII	1200 (1/2)	10	2000	26.5	100
VIII	2000 (1/2)	10	1170	26.2	70

Note. — Columns are: survey name for text reference, survey area in square degrees, survey time in months, total exposure time in each optical band in seconds, 10σ galaxy flux limit in I-band (using AB magnitudes), source galaxy number per square arcmin (estimated number useable for weak lensing—the number useable for photometric redshifts is generally comparable). The lower 3 choices assume only half the optical passbands are observed for each object; this requires less survey time per unit area, but at the cost of somewhat reduced photometric redshift accuracy. In all cases, 85% observing efficiency (due to data downloads, calibration, etc) is assumed (Rhodes et al. 2003). Last 2 columns are estimated from Massey et al. 2003. From the shallowest (III) to the deepest (II), the mean source galaxy redshift only varies from about 1.16 to 1.3. For reference, the total co-added exposure time per optical filter in the SNAP Deep (Supernova) Survey is estimated to be 144,000 sec.

In estimating the survey parameters, we follow (Rhodes et al. 2003) etal in assuming 85% observing efficiency (due to downtime for data downloads, calibration exposures, and passage through radiation belts). The area SNAP can survey in N_m months through N_f optical filters, assuming on-board data storage and transmission issues can be solved by compression, is

$$A(N_m) = \frac{31,212 N_m}{[(t_e/\mathrm{sec}) + 20]} \left(\frac{6}{N_f}\right) \left(\frac{4}{N_{\mathrm{exp}}}\right) \text{ sq.deg.}$$

where t_e is the single-frame exposure time, 20 sec is the design overhead for CCD readout and telescope slewing between exposures, and N_{exp} is the number of exposures in each optical filter per field. We assume $N_{\mathrm{exp}} \geq 4$ in order to reject the cosmic ray background. For example, for 500 sec exposures and a survey of 5 months, this yields a 300 sq. deg. survey. Note that the exposure time in Table 2 is the total exposure time on a field.

We also consider strategies that do not employ all the filters to learn about tradeoffs of area versus photo-z precision. Figure 3 shows the layout of the SNAP focal plane. The fiducial scan strategy is to make 4 small dithers at each telescope pointing followed by a set of shifts equal to the width of one of the optical filters until each source is covered by all 9 filters (8 times in each NIR filter, 4 in each optical filter). The alternative '1/2' strategy shifts over twice as far, so each object is covered in only 3 of the optical filters. Because of the CCD layout, this results in a checkerboard pattern of optical coverage. This will result in reduced precision in photometric redshifts.

The strongest option developing from our study is a 1000 sq-degree survey consuming 10 months of telescope time to a depth just 0.3 magnitudes brighter than the default 300 sq-degree survey. This option is designated "fidicual" and is number V in our matrix.

3. Cluster Abundance: Optical/IR Cluster Counts and the Growth Function

The chief scientific goal of the SNAP mission is the study of dark energy. A weak lensing survey, complementary to the supernova program, has been an integral part of the SNAP mission (Kim et al. 2002), with a significant fraction of the mission devoted to a wide area survey tailored to this goal. It is just this wide area survey which many researchers at Fermilab are most interested in. In this section we describe the cluster counting technique, why SNAP is so well suited for it, and what one can learn from it. We also discuss how to optimize the wide area survey for study of dark energy with cluster counting.

Cosmology with galaxy clusters– Galaxy clusters are the largest gravitationally bound objects in the universe, and they can be identified over a wide range of distances, which makes them attractive objects to use as cosmological probes. Galaxy clusters form from small density perturbations in the early universe that are gravitationally unstable and eventually collapse to form bound, virialized systems. The growth of clustering is hierarchical, with small clusters forming first and large clusters later. The rate at which clusters can grow depends on the fractional amount of dark energy in the universe at any time - in a universe dominated by dark energy, the growth of structure is slower than in one dominated by matter. In the past the universe was dark matter dominated, and cluster formation was vigorous. The equation of state of dark energy determines how long this phase lasts. For example, the redshift at which dark matter was 70% of the total density (versus its current 30% today) is 0.7 if $w = -1$ but is 1.5 if $w = -0.6$. The dependence of growth rate on dark energy has a direct impact on the number of galaxy clusters that we see as a function of redshift, as does the effect of dark energy on the relationship between redshift and distance to a cluster. SNAP will be able to detect clusters to redshifts of 2 and higher and will sample the universe at the time of transition from dark matter to dark energy domination. The dependence of the number of clusters as a function of redshift will reflect the signature of this transition.

Galaxy clusters are most easily detected by optical means, but they can also detected by other techniques by virtue of their being filled with a hot, ionized gas at a temperature of order 10^8 K. This gas can be detected at Xray energies by measuring the thermal emission from the gas or at radio wavelengths by observing the distortion of the microwave background due to electron scattering as microwave photons pass through the cluster gas (an effect known as the Sunyaev-Zel'dovich effect). Both techniques have been proposed as the basis of experiments to count galaxy clusters to high redshift and measure cosmological parameters, including w (Wang & Steinhardt 1999; Haiman et al. 2001; Levine et al. 2002). We propose that one can alternatively use optical methods to detect and count clusters. Optical techniques have largely been ignored in the past due to difficulties in cleanly identifying clusters as one goes to high redshift. We will show that by using the high quality photometry from SNAP not heretofore considered, one can detect clusters much more cleanly than previously assumed, and that optical techniques offer advantages over the Xray and SZ methods.

In the next section we outline the basis for the experiment. In the following section we describe the experiment in more detail. In the succeeding sections we compare the advantages and disadvantages of the optical, Xray, and SZ experiments relative to each other.

3.1. The Experiment

Theoretical Basis– The most straightforward way to characterize a distribution of galaxy clusters is to construct a cluster mass function that is a function of redshift: $dN/dMdz$, where N is the number of clusters per mass M and per redshift interval z, integrated over some area of the sky. The classic theory for predicting this function is due to Press & Schechter (1974), who derive an expression for this function in a scale-free hierarchically clustering universe. This theory makes a number of simplifying assumptions to bypass the complex processes involved in nonlinear dynamics, but it does provide physical insight into the cluster formation process. At a fixed time, the mass function is characterized by a power law in mass for low mass clusters and an exponential fall-off for high mass clusters, with a characteristic mass M_* that has a collapse time of order the age of the universe at that time. As the universe evolves, the shape of the mass function stays the same but M_* shifts to higher mass. The magnitude of the shift depends on w, Ω_{DM} (the fraction of density today in dark matter) and Ω_0, the total density of the universe today. To keep the discussion tractable we will assume that the latter two parameters are constrained by other observations of the cosmic microwave background and the local universe. In practice one can also measure Ω_{DM} from the cluster counts.

The Press-Schechter function falls somewhat short in matching the clustering process predicted by n-body simulations, mainly in that it overpredicts the number of low mass clusters and underpredicts the number of high mass clusters. Jenkins et al. (2001) have carefully analyzed clusters produced in a series of simulations and derived a more accurate function that better describes the mass function. This function retains the property of the Press-Schechter function that it depends on a single scale mass:

$$\frac{dn}{d\log M} = -0.315 \frac{\rho_c \Omega_{\mathrm{m},0}}{M\sigma_M} \frac{d\sigma_M}{d\log(M)} e^{-|0.61 - ln(D_z\sigma_M)|^{3.8}} \tag{7}$$

where n is the space density of clusters in the range $log(M)+dlog(M)$, M is the mass of the cluster, ρ_c is the critical density, $\Omega_{\mathrm{m},0}$ is the total mass density of the universe in units of critical at $z = 0$, σ_M is the variance of mass on scales of mass M, and D_z is the linear growth function.

We do not observe the density of clusters directly, but rather the number of clusters per increment in redshift Δz. There is sensitivity to w in this conversion of n from Mpc^{-3} to a surface density as it requires knowing the volume between two redshift shells:

$$V = \frac{c}{H_0} \int_{z_1}^{z_2} r^2(z)/H(z)dz \tag{8}$$

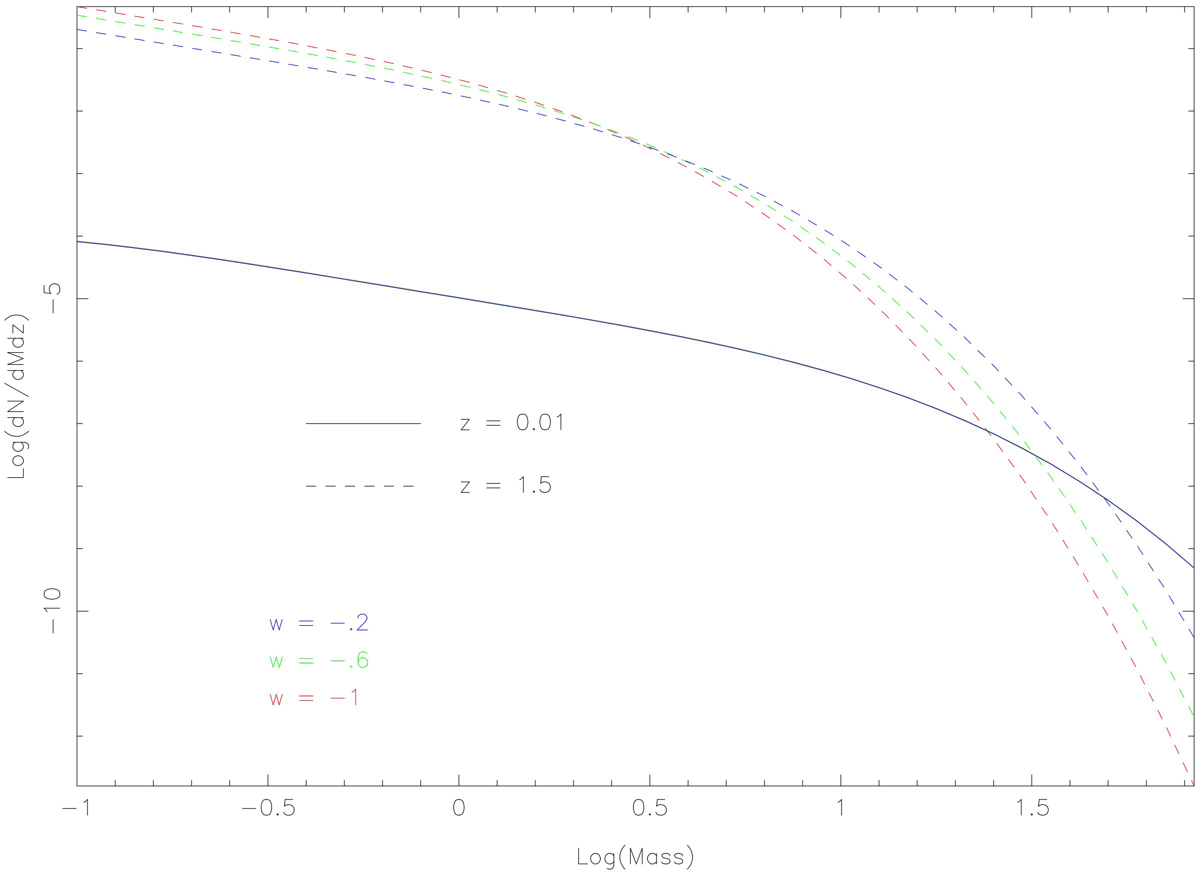

[]

Fig. 4.— Mass function of galaxy clusters versus redshift for two different redshifts and three different values of the parameter w

The combined effects of cluster growth and volume element dependence on w determine the properties of the cluster mass function. Figure 4 shows mass function predictions at $z = 0$ and for three values of w at $z = 1.5$. The main effect of changing w from -1 to -0.2 is that the number of low mass clusters decreases and the number of high mass clusters increases at high z.

The current value of M_* is estimated to be $2.7 \times 10^{13} h^{-1}$ $M_\odot$, where h is the current value for the Hubble constant in units of 100 km s^{-1} Mpc^{-1}.

Data set– SNAP will produce two major datasets: the deep survey, that repeatedly images two 7.5 square degree fields for the supernova search, and the wide field survey, that will cover an area of 300 square degrees to a depth slightly greater than that of one pass of imaging of the deep survey. We will use the wide field survey for counting galaxy clusters. The baseline plan for the wide field survey calls for imaging a set of fields in each of the 9 SNAP filters with an exposure time per filter of 2000 seconds, longer than the 1200 seconds per exposure of the supernova survey. These exposures will detect point sources to AB[5] = 28 (5σ) and galaxies to AB = 26.5 (10σ).

Cluster detection– The imaging data will be processed to provide a catalog of stars and galaxies with parameters that include positions and fluxes in all 9 filters. At the sensitivity of SNAP, it is expected that the vast majority of objects will be galaxies. The galaxy catalog will be analyzed using the maxBCG technique to create a catalog of galaxy clusters. The maximum redshift to which galaxy clusters can be detected depends on both the limiting sensitivity of the experiment and the wavelength coverage.

The maxBCG technique is described in detail in section 9.2, and only a summary is presented here. The technique relies on two properties of galaxy clusters: first, the brightest galaxy in the cluster (BCG) has a luminosity and a color that is roughly the same in every cluster (there is a population dispersion of 0.5 magnitudes in luminosity and 0.04 magnitudes in color), and second, there is a population of red galaxies that all have the same color as the BCG (after taking into account a small color-luminosity relation). Given these two facts, one can search for clusters in a galaxy catalog by calculating the likelihood that any given observed galaxy could be a brightest cluster galaxy at redshift z just by predicting the magnitudes and colors of the mean population redshifted to that z, and by looking for the red population at that z about the candidate. A side product of the cluster search are two very useful quantities: a very precise and accurate photometric redshift (accuracy of ≈ 0.015) and a count of the E/S0 galaxies in the cluster, N_{red}, which scales with mass. Figure 5 shows a picture of a rich cluster, illustrating the uniformity of color of the vast majority of its members. Figures 6 and 7 illustrate just how much more information there is in space based images.

---

[5]AB is a magnitude system as opposed to a filter, such as R. Here AB indicates that any filter in the AB system through which an object has as the given magnitude and which is used by SNAP will have the given S/N

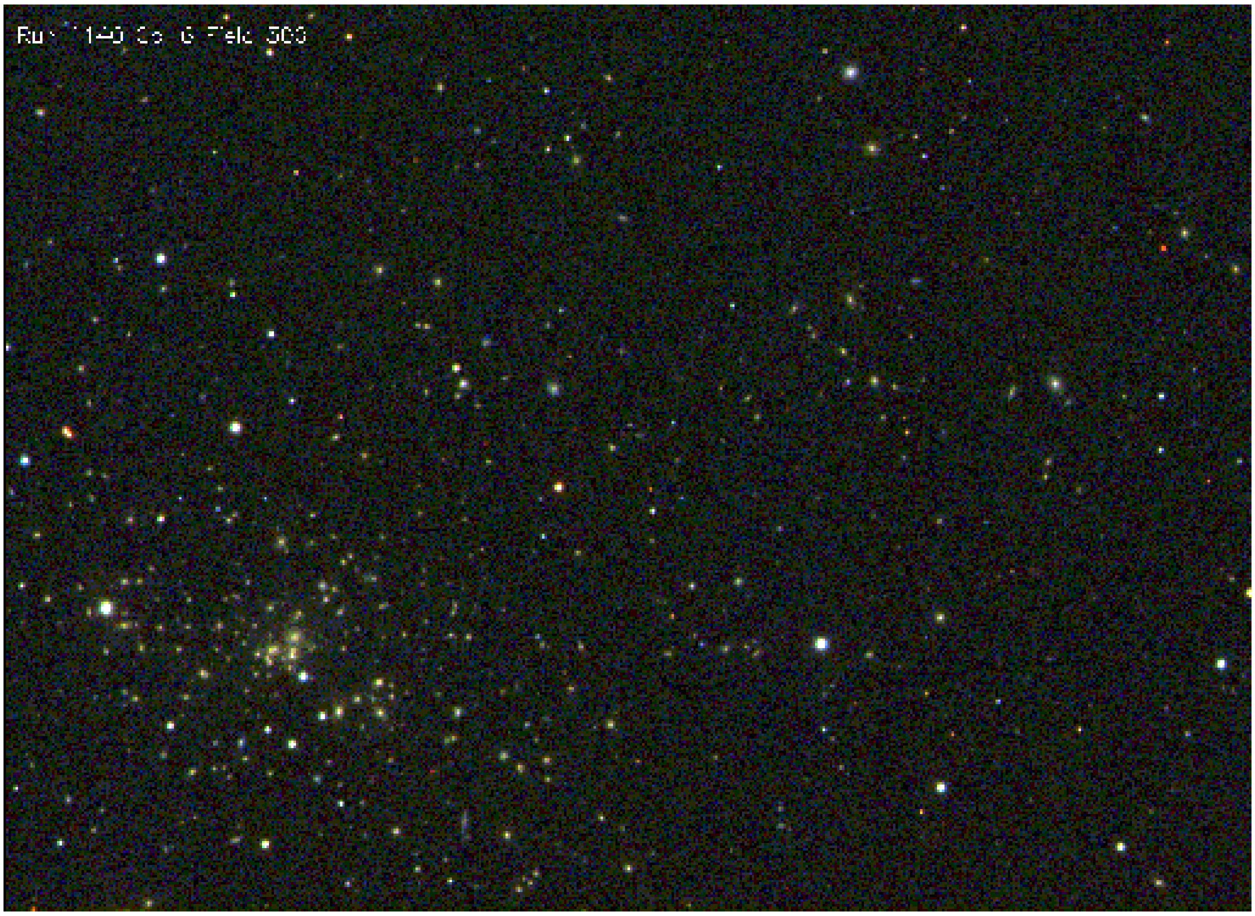

Fig. 5.— Image of the galaxy cluster Abell 1689. Note the large number of galaxies of uniform color. This is a full SDSS image, 0.22 degree x 0.15 degree.

The maxBCG technique will be tailored to best utilize the SNAP filter set. The reference filter, in which fluxes are measured, must be completely longward of the H+K break in the elliptical galaxy spectrum at about 4022 Å. Based on an analysis done with a preliminary prescription for the SNAP filter set, we find that the maximum redshift meeting this condition is 2.4.

The limiting flux is set by the condition that we wish to measure colors to high accuracy, 3% or better. The intrinsic spread in colors of red cluster galaxies is known to be extremely small (4% or less, Bower, Lucy, & Ellis (1991)), so accurate colors allow one to identify and measure the content of clusters more precisely. For computational purposes we measure the color using two SNAP filters that, in the rest frame of the galaxy, fall on either side of the H+K break at 4022 Å. The S/N ratio of the color measurement is dominated by the short wavelength filter, and a simple calculation shows that the S/N ratio of the flux measurement in this band should be at least 40.

The S/N ratio has been computed for a 1/2 L_*[6] galaxy (the faintest object measured by maxBCG) using standard parameters for the SNAP telescope and detectors and a $w = -1$ cosmology. The luminosity of red galaxies is known to evolve in time (Schade et al. 1999). For this calculation, it is assumed that galaxies increase in brightness by 1 magnitude to a redshift of 1 but are constant after that; the exact dependency for higher redshifts has not been measured yet, and the assumption of constant brightness is likely pessimistic.

The apparent magnitude and S/N ratio at different redshifts is shown in Table 3 for two sets of exposure times corresponding to the deep and wide surveys.

Calibration– Theoretical models and simulations of the universe track mass, which is primarily in the form of collisionless dark matter whereas the maxBCG technique detects galaxies. The relationship between the two is not straightforward: galaxies form from dissipative baryonic matter and thus tend to sit at the centers of halos of dark matter. Not all baryons form galaxies: in clusters, the process of cluster formation causes much of the baryonic matter to heat through shock collisions to a temperature of 10^8 K, preventing it from coalescing into galaxies. Galaxies are not standard candles: they evolve in time, mainly dimming and becoming redder as star formation ceases. The conversion between N_{red} and total cluster mass must be calibrated. This will be achieved by measuring the weak lensing distortion of background galaxies behind each of the clusters detected by the maxBCG method. The weak lensing signal is proportional to the cluster mass. A weak lensing experiment to measure cosmic shear is itself a principal goal of the wide field survey, and the accuracy needed to measure cluster masses is much less than that needed for the shear-shear measurements that the weak lensing experiment will itself measure.

Figure 8 shows the results from the SDSS survey calibrating the relation between N_{red} and

[6] $L_\star$ refers to the characteristic galaxy luminosity in a Schechter function fit (power law plus exponential high-L cutoff) to the luminosity distribution. M31 is about an $L_\star$ galaxy, the LMC is $< 0.5 L_\star$.

Table 3. Galaxy Cluster Sensitivity Limits. ($w = -1$)

Redshift	Apparent Magnitude (blue filter)	Signal/Noise (1170 sec exposure)	Signal/Noise (2000 sec exposure)
0.5	21.4	163	214
1.0	22.5	88	116
1.5	23.3	53	71
2.0	23.9	45	60
2.4	24.2	35	45

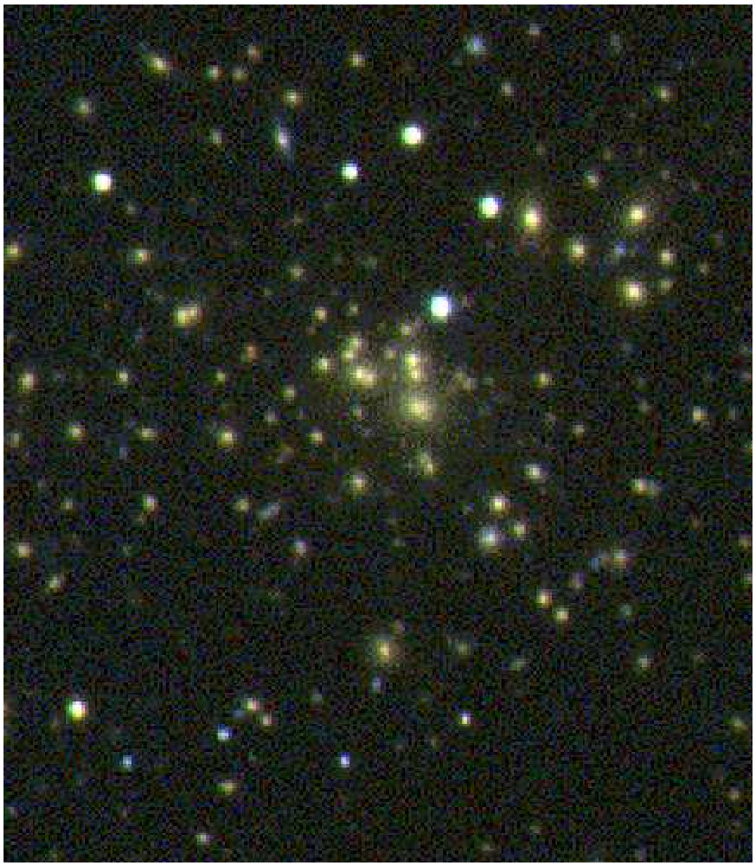

Fig. 6.— A cutout of the core of A1689 from the the SDSS image. This is the same scale as in figure 7

a parameter that measures cluster mass for nearby clusters. The calibration is expected to be a function of redshift, so the SNAP data will be analyzed to determine this function. It should be noted that other experiments to measure dark energy, aside from the weak lensing experiment itself, do not have the capability of calibrating their "standard candle" (be it supernovae, Xray temperature, or SZ decrement) as a function of redshift.

It is worth noting that the various bins in figure 8 have roughly constant signal to noise. This can be shown to be generic: in a weak lensing program where one stacks all the objects from a given mass bin, the signal and noise are

$$S \propto M \text{ and } N \propto \#_g^{-1/2} \tag{9}$$

where $\#_g$ is the number of background galaxies. Now, $\#_g \propto \#_c r^2$ where r takes into account the fact that less massive clusters are smaller. This size may be estimated via virial relations: $r \propto \sigma$, and the mass of a cluster $M \propto \sigma^3$ (e.g., Borgani et al (2001)). The number of clusters $\#_c$ we know from maxBCG investigations to be $\#_c \propto N_{red}{}^{-3.5}$, in linear binning. We can take $M \propto N_{red}$ without

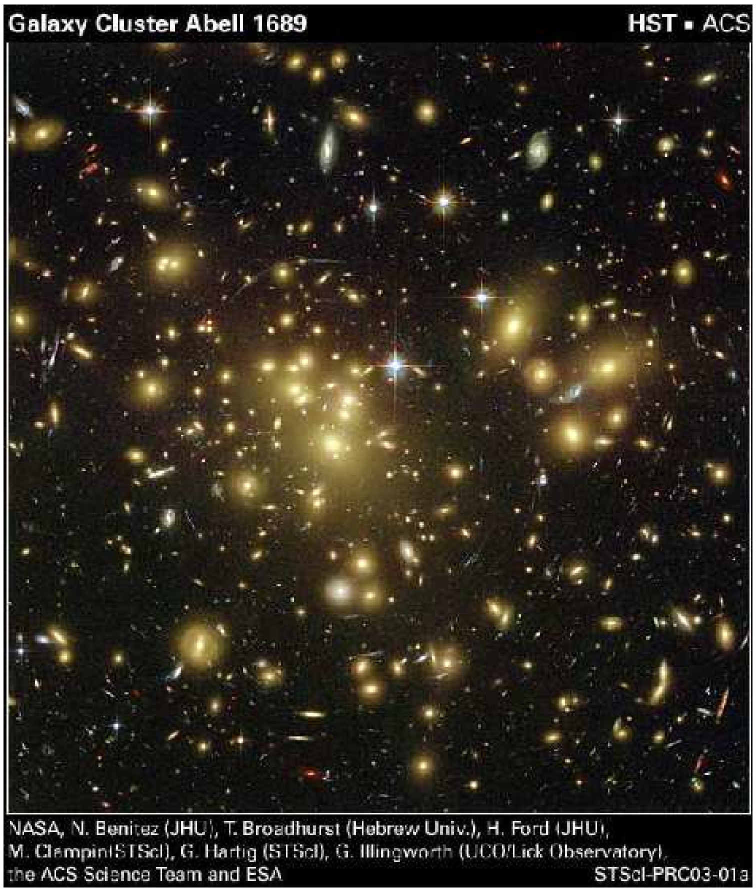

Fig. 7.— An image of the core of A1689 taken with HST. This image has depth and resolution comparable to that SNAP will achieve, and is at the same resolution as in figure 6. (HST courtesy of NASA and the PI, N. Benitez.)

being far wrong, leading to:

$$\#_g \propto \#_c r^2 \propto M^{-3.5} M^{2/3} \propto M^{-2.8}, \tag{10}$$

and thus to

$$S/N \propto M/\#_g^{-1/2} \propto M/M^{1.4} \propto M^{-0.4} \tag{11}$$

This weak dependence on M is the suggestion that measurements of the mean cluster in a N_{red} bin will have roughly constant signal to noise across the range of N_{red}. It took about 30,000 background galaxies spread over areas corresponding to circles of radii 1 Mpc at the cluster to to make an accurate weak lensing measurement on the 42 $z \approx 0.15$, $10^{14} M_\odot$ SDSS clusters in Sheldon et al. (2001). In the SNAP Wide Area Survey the surface density of galaxies with photo-z indicating $z > 2.5$ is ≈ 14 galaxies/sq-arcminute, so at our limit of $z = 2.4$ would require about 40 clusters of the same mass to achieve the same signal. This suggests that a) we will be able to calibrate the

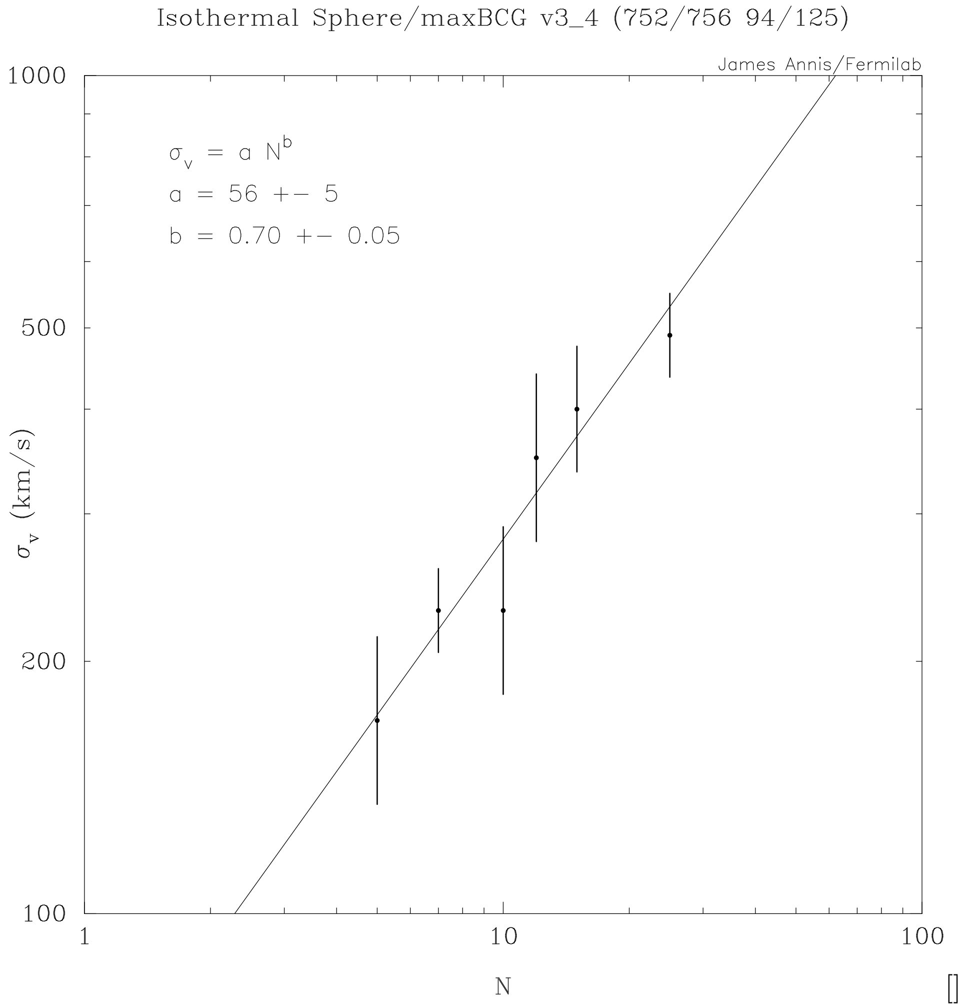

Fig. 8.— Calibration of cluster mass measured by weak lensing vs. number of galaxies counted by maxBCG. The mass of a cluster is parameterized by the velocity dispersion of an isothermal sphere; the mass is defined to be that which is inside the radius where the mean interior density is 200 times the critical density of the universe. The data for this plot are from Tim McKay's Michigan group.

N_{red}-mass relation at the high mass end at $z = 2.4$, and thus that we will be able to calibrate the N_{red}-mass relation over the entire N_{red} range and for all z at $0.2 \leq z \leq 2.4$.

Analysis– Figure 9 shows an analysis of cluster counts from a portion of the SDSS survey and illustrates how the different steps described above are combined.

A full analysis of the SNAP data will be done using a maximum likelihood technique and has not been simulated yet. However, the main sensitivity of the wide area survey to dark energy comes through the effect of w on the number of high mass clusters as a function of z. If one could calibrate observations cluster masses perfectly, it would be straightforward to compare counts of clusters at low and high redshift. However, the accuracy of the estimate of w depends sensitively on errors in the mass calibration. For example, if one counts clusters more massive than $8M_*$ (which are typical of Xray clusters), an error in the mass calibration of 10% produces an error of 0.3 in the estimate of w. The technique used here is to count the clusters into two mass bins and compute the ratio $R = \log[N(M_0 < M < M_1)/N(M_1 < M < M_2)]$, which roughly measures the logarithmic slope of the high end of the mass function. This ratio is then averaged over two redshift ranges, and the difference of the two $P = R(z_0 < z < z_1) - R(z_1 < z < z_2)$ is the parameter used to estimate w.

Table 4 list the number of clusters that are expected for different masses and cosmologies in two mass and redshift ranges and the parameter P for a 300 square degree survey. The two mass ranges are $2M_* < M < 5M_*$ and $5M_* < M < \infty$, and the two redshift ranges are $0.5 < z < 1.2$ and $1.2 < z < 2$.

Table 5 give the errors in estimating w from P. Calculations have been done for both 300 and 1000 square degree surveys. Statistical errors are 1σ.

Systematic Errors– Table 5 shows that in principle one can make an accurate measurement of w using galaxy cluster counts. However, this accuracy may be lost if systematic errors are not controlled.

Table 4. Galaxy Cluster Counts

w	Low-z counts		High-z counts		P
	N_1	N_2	N_1	N_2	
-1.0	24596	3235	15655	751	-1.01
-0.6	20464	3049	16949	1092	-0.84
-0.2	15347	2678	15536	1488	-0.60

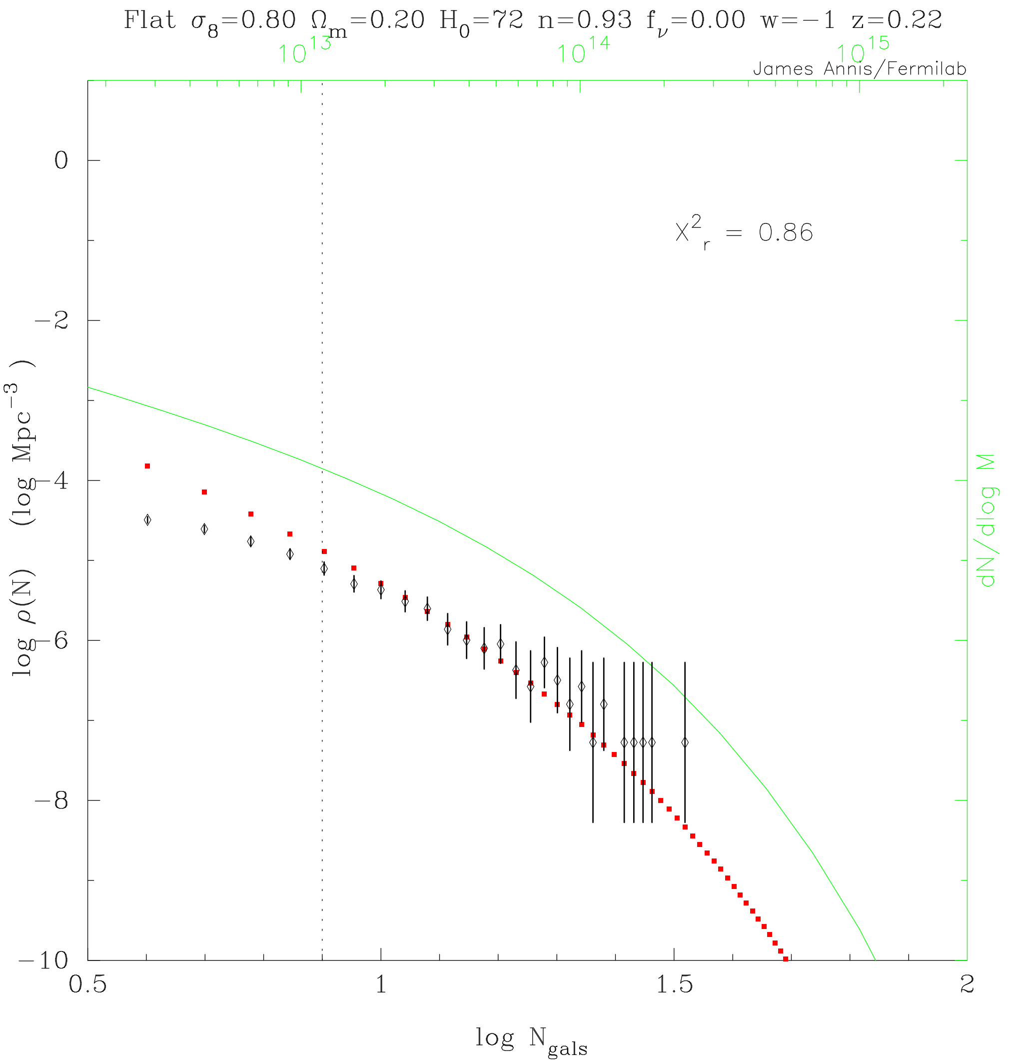

Fig. 9.— An example of the program for 392 square degrees from the SDSS. Plotted here is the number function, the number of clusters as a function of N_{red} (on the plot denoted N_{gals}), in the redshift shell $0.1 \leq z < 0.25$. The dotted red line is the prediction, the points with error bars are the data. The solid green line is the Jenkins mass function, to be referred to the top axis. The thin dotted vertical line is the lower limit to which clusters are included in the χ^2 fit. Below that one is clearly incomplete, either because of the algorithm, or because Nature does not produce halos with red galaxies at those masses. The best fit cosmology is at the top of the plot.

The first systematic error has already been discussed - that due to an offset in the calibration of N_{red} vs. mass between low and high redshift. A 10% error leads to an 8% error in w. Experience with SDSS calibrations of low redshift clusters using weak lensing suggests that this is a reasonable error to expect.

A second systematic error involves the details of the maxBCG technique itself, which technically requires a knowledge of cosmology in order to count galaxies in a cluster, since they are counted inside a metric radius to a predictable limiting magnitude, but the radius and limiting magnitude are a function of cosmology. The standard technique is to correct the counts iteratively as part of the process of measuring the cosmological parameters. (Historically, for measuring the brightnesses of galaxies, this correction has been called the "aperture correction").

Galaxies evolve in brightness and color with redshift, so the relation between N_{red} and mass will change. This is in principle taken care of by the weak lensing calibration, but it adds an extra dimension of uncertainty.

Finally, the identification of clusters via optical techniques suffers from the imprecision with which clusters can be identified. Even in n-body simulations, clusters are not crisply identifiable entities, since the simulations show that mass is clustered hierarchically on all scales. This in fact points to a very useful technique: if the simulations are good enough, one can run the cluster finding algorithm on them just as one does on the real data. This is a very good way of understanding just what it is finding. One must use algorithms that do the "best job possible" and apply them uniformly to both the observation and the simulations in order to make meaningful comparisons.

3.2. Comparison with Other Cluster Detection Techniques

Since the Xray and S-Z methods have received the most attention in the literature, it is informative to compare the strengths and weaknesses of these methods vs. optical detection of clusters.

The main strength of the Xray and S-Z methods is that they only detect the hot gas in the centers of galaxy clusters. This hot gas only exists in the highest density regions that have collapsed

Table 5. Errors in w

	w error
300 sq. deg. survey	0.091
1000 sq. deg. survey	0.051
10% mass calibr. error	0.083

and virialized. Such regions are easily identified both observationally and in simulations that include hydrodynamics. Optical methods, by contrast, are sensitive to all galaxies and structures, including those that have not yet virialized or that are members of small groups that, in Xray or S-Z, would be too cool to detect. The maxBCG method focuses on only red galaxies, which are known to be found primarily in the same regions as the hot gas (implying that the two have a related origin) but red galaxies are also found outside of these regions. Because optical methods see more of the "flotsam and jetsam" of the universe, they are sensitive to errors induced by projection effects, whereby chance alignments of galaxies along the line of sight are mistaken for galaxy clusters. The maxBCG method takes an enormous step forward in reducing the impact of projection effects by using color as a redshift indicator. Simulations will need to be done to determine if errors due to projection effects still linger or are negligible.

The main strength of the optical method is that it is able to detect clusters of much lower mass than the Xray/SZ techniques, and with SNAP, which means that it will be much less sensitive to selection biases that the other techniques must understand in great detail. Second, optical techniques immediately measure the redshift of a cluster, whereas the other two techniques require followup observations (and would greatly benefit from a SNAP-like survey!). Finally, while the S-Z survey can detect clusters almost independent of redshift, an Xray survey using projected future technology is still limited to detecting clusters to redshift 1, and then only the most luminous such objects.

Formally, the optical cluster counts presented here give the strongest constraints on w. However, all three methods are dominated by systematic errors, and these have not been explored at the level of detail needed to show the superiority of one over the other.

4. Weak Lensing

The weak lensing survey component of SNAP is of interest to researchers at Fermilab for its stated purposes of weak lensing as well. In this section we describe the weak lensing technique, why SNAP is so well suited for it, and what one can learn from it. We also discuss how to optimize the wide area survey for study of dark energy with weak lensing.

4.1. Weak Lensing: What Is It and How Does It Work?

It has been known for nearly a century that light is bent by a non-uniform gravitational field. This effect has been applied to the images of distant galaxies in order to determine the distribution of mass between the source an observer on earth. Strong lensing results in severe and obvious distortions of the source, possibly including multiple images or long arc-like images. Weak lensing is characterized by small distortions in shape and and sizes of galaxy images. Since the properties of galaxies are only known on average, weak lensing studies the statistical properties of a large number of galaxies in order to determine statistical or average properties of the projected mass. The effects of image distortions can be divided into *magnification*, *rotation*, and *shear*. There is no method to measure rotation, and although measurement of magnification is possible and can yield comparable information to shear, we will here only discuss shear measurements, which have proved themselves with many successful detections. The SNAP mission is especially well suited to measure weak lensing shear because of its ability to see a large number of distant galaxies with good imaging resolution over a large area of the sky. The capabilities of SNAP for weak lensing have been explored by the SNAP collaboration in a series of papers [Rhodes et al. (2003); Massey et al. (2003b); Refregier et al. (2003b)].

Weak lensing theory– Experimentally, weak lensing is performed by selecting a large number of galaxies that are bright enough and extended enough so that they we can accurately measure the surface brightness pattern, $B(\vec{x})$, where $\vec{x} = \binom{x_1}{x_2}$ is the position on the sky. A commonly used and compact notation is to use complex number to represent the position on the sky ($x = x_1 + ix_2$) as well as other quantities. One then measures the (complex) 1st and 2nd central moments of the brightness distribution for each galaxy:

$$\bar{x} = \int d^2\vec{x}\, x\, B(\vec{x}) \quad M_2 = \int d^2\vec{x}\, (x - \bar{x})^2 B(\vec{x}) \quad M_0 = \int d^2\vec{x}\, |x - \bar{x}|^2 B(\vec{x}) \ . \tag{12}$$

These moments define a complex *ellipticity*: $e = M_2/M_0$, which has two components $e_1 = \mathrm{Re}[e]$ and $e_2 = \mathrm{Im}[e]$. A galaxy's scalar ellipticity, $|e| = \sqrt{e_1^2 + e_2^2} \in [0, 1]$, is zero for a circular galaxy image and unity for a "linear" galaxy, such as an edge on spiral. A graphical illustration of ellipticity is given in figure 10. Note that the orthogonal direction of ellipticity corresponds to rotating the galaxy by 45°, in contrast to rotation by 90° which corresponds to multiplying by -1.

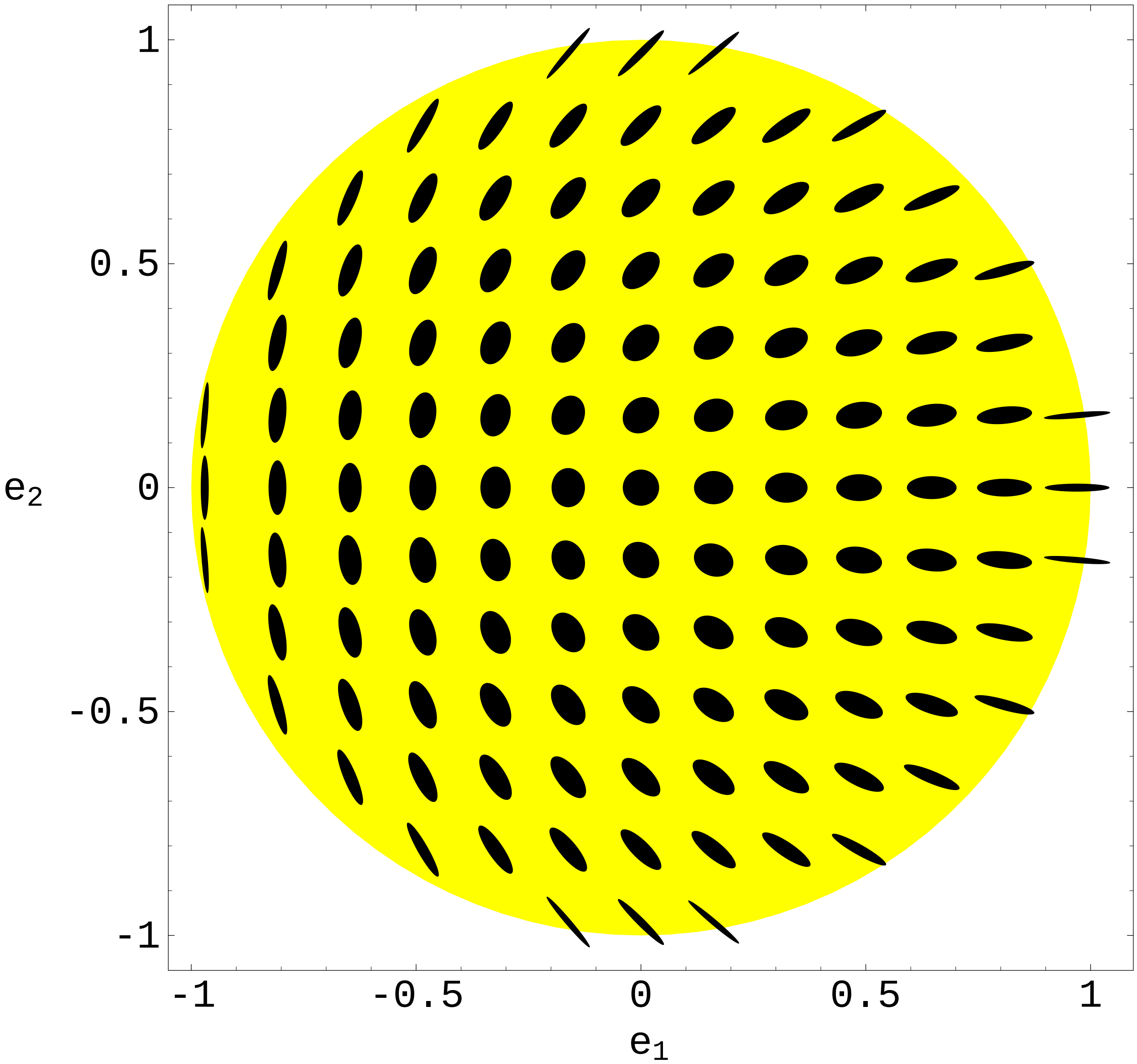

Fig. 10.— An array of ellipses with ellipticity given by e_1 and e_2 values at their position.

Gravitational lensing causes the images of galaxies we see (image on the *image plane*) to be a distorted from what one would see if there were no lensing (image on the *source plane*). The angular gradient of the lensing deflection angle vector in the sky is called the *deformation tensor* and the shear is its traceless symmetric part. The shear has two components and can also be written a complex number, γ. If galaxy shapes are are randomly oriented then one effect of the lensing shear is to cause an alignment in the lensed (i.e. observed) ellipticities. This alignment can be expressed in terms of a non-zero expected ellipticity, given by $\langle e\rangle = P_{\rm sh}\gamma$ where the proportionality constant, $P_{\rm sh}$, is called the *shear polarizability.*

We can try to use the measured ellipticities to infer the the shear, constructing an estimator $\hat{\gamma} = e/P_{\rm sh}$ for each galaxy. If the shear is small then $P_{\rm sh} = 1 - \frac{1}{2}\langle |e|^2\rangle \simeq 1$ since galaxies typically have a moderate ellipticity, $\langle e^2\rangle \approx (0.3)^2$. From the measurement of a single galaxy shear estimator has an error

$$(\Delta\gamma)^2 = \langle |\hat{\gamma} - \gamma|^2\rangle = \frac{\langle |e|^2\rangle}{P_{\rm sh}} \simeq (0.3)^2 \tag{13}$$

The error is known as *shape noise.* The shape noise is ideally uncorrelated between galaxies so one can determine the average shear more accurately using many galaxies, the error going like $\delta\gamma \approx 0.3/\sqrt{\#_{\rm g}}$, where $\#_{\rm g}$ is the number of galaxies used. Since typically $\gamma \lesssim 10^{-2}$ one needs ellipticity measurements from $\gtrsim 10^3$ galaxies to detect the shear with S/N of 1.

To quantify the shear pattern one computes (theoretically) or estimates (observationally) either 2-point correlation functions or angular power spectra, here we discuss the latter. One can construct 3 geometrically different versions of these, one is zero because of parity invariance, and the remaining two are related by rotating the shear by 45°, and are sometimes called “E-modes” and “B-modes”. If density inhomogeneities produce the shear, as we expect, then the expected B-mode amplitude is much smaller than the expected E-mode amplitude, and the former provides an excellent probe of both shape noise and systematic errors. An estimator, $\hat{C}_l$, for the E-mode power spectrum is the final product and this should be compared to it's theoretical expectation value, $C_l = \langle \hat{C}_l\rangle$ to infer properties of our universe.

The expected shear angular power spectrum is given by (for $l \gg 1$)

$$C_l = 18\pi^3\Omega_{\rm m,0}^2\,\frac{H_0^3}{c^3}\int_0^\infty dz\,(1+z)^2\,\frac{H_0}{H(z)}\beta(z)^2\,P(\frac{l}{D_{\rm A,co}(0,z),z)},z)\ . \tag{14}$$

Here z gives the redshift, $\Omega_{\rm m,0}$ parameterizes the present dark matter density, $H(z)$ gives the cosmological expansion rate (Hubble parameter) as function of redshift; $H_0 = H(z=0)$; $P(k,z)$ is the power spectrum of dark matter inhomogeneities as a function of comoving wavenumber and redshift; and $\beta(z) \in [0,1]$ is the lensing efficiency. The comoving angular diameter distance, $D_{\rm A,co}(z_1,z_2)$, indicates how far and object at redshift z_2 appears to an observer at redshift z_1 according to the it's angular size. The smaller the angular size the further away it appears, the larger is $D_{\rm A,co}(z_1,z_2)$. The lensing efficiency is determined by the redshift distribution of galaxies used to measure the shear via the equation

$$\beta(z) = \frac{1}{N_{\rm g}} \int_z^\infty dz_{\rm g} \, \frac{dN_{\rm g}}{dz_{\rm g}} \, \frac{D_{\rm A,co}(z, z_{\rm g})}{D_{\rm A,co}(0, z_{\rm g})}. \tag{15}$$

Note that $\beta(0) = 1$ but since galaxies are concentrated at low z it falls off rapidly. A *deeper* weak lensing survey, one which includes dimmer galaxies which are further away, will fall off less rapidly, leading to larger $\beta(z)$ and larger shear (larger C_l).

A weak lensing survey which covers a fraction, $f_{\rm sky}$, of the entire sky can determine the angular power spectrum in a band of width Δl to an accuracy

$$\frac{\Delta C_l}{C_l} = \frac{1}{\sqrt{l \, \Delta l f_{\rm sky}}} \left(1 + \frac{C_l^{\rm sn}}{C_l}\right) \qquad \text{and} \qquad C_l^{\rm sn} = \frac{(\Delta\gamma)^2}{2 \, N_{\rm g}} \tag{16}$$

where $C_l^{\rm sn}$ is the shape noise spectrum determined by the number of galaxies per steradian $N_{\rm g}$ and the shear error from one galaxy, $\Delta\gamma \approx 0.3$. The $f_{\rm sky}$ dependence gives the sample variance, i.e. how well one has sampled the expected distribution of shears. It is the cosmological average statistics, and not local values which fluctuate, which give the physical parameters which describe our universe.

For shallow surveys the shape noise term dominates and one decreases this noise by increasing the number of galaxies with deeper exposures, which has the added benefit of increasing the signal because the galaxies are further away. Once the survey gets deep enough that the signal-to-noise is greater than one, the uncertainty, ΔC_l, saturates due to sample variance and one must increase the area covered to improve the measure of cosmological parameters. Thus one must go both wide and deep in order to maximize the cosmological information from a weak lensing survey.

Why is SNAP Good at Weak Lensing?– SNAP makes an excellent weak lensing probe because it has the capability for an imaging survey which is both very deep and very wide. This is illustrated in table 6 where one sees that both the galaxy density and area of the survey will be increased by about an order of magnitude over that which is typical of recent detections of shear-shear correlations. It is worth noting that this table hides information about the extent sample variance limits the accuracy and the extent to which uncertainties in the redshift distribution in the background galaxies affect the measurement. The approach to the latter that SNAP will take is photometric redshifts, to which it is particularly well suited for accurate photometric redshifts, particularly because of the IR bands have very high backgrounds in ground based observations.

Weak lensing has always been a *relatively* imprecise cosmological probe. For example the accuracy with which weak lensing can measure shear (i.e. mass) correlations is always less than that which similarly sized surveys can measure galaxy correlations simply because the shear in magnitude is much smaller than the fractional density contrast: $\gamma \ll \delta\rho/\bar{\rho}$. The advantage of weak lensing is that what it measures, mass, is more accurately predicted by theory than the galaxy distribution. We see from fig 11 that even with it's intrinsic limitations that a SNAP wide area

Reference	**Survey Area** $[(^\circ)^2]$	**Galaxy Density** $[\text{gals}/(^\circ)^2]$	**Significance**
(Bacon et al. 2000)	0.5	5×10^4	3σ
(Wittman et al. 2000)	1.5	9×10^4	5σ
(Van Waerbeke et al. 2000)	1.7	9×10^4	5σ
(Wilson et al. 2001)	1.5	8×10^4	5σ
(Van Waerbeke et al. 2001)	6.5	6×10^4	12σ
(Jarvis et al. 2002)	75	3×10^4	4σ
SNAP deep	15	9×10^5	45σ
WAS default	300	4×10^5	200σ
WAS fiducial	1000	3×10^5	350σ

Table 6: A comparison of existing weak lensing surveys with what can be expected from a SNAP weak lensing survey. The galaxy densities are for galaxies usable for weak lensing. The "WAS default" survey listed here is for the default SNAP 300 sq-degree survey strategy. We see that SNAP brings weak lensing into a regime where it can be used as a very precise measure of cosmology.

survey will make weak lensing a very precise probe of cosmology, on par with what is presently available from CMBR anisotropy studies. Since, in contrast to CMBR, weak lensing primarily probes a much lower redshift range, it is a complementary probe and much more sensitive to dark energy which only make its presence known at low redshifts.

Dark Energy and Cosmological Parameters– At the largest scales the average luminosity-redshift relation probes the propagation of a light beam across the universe and is effected by the mean density and pressure of the cosmological material. This is the effect used to infer the dark energy from the shift in Type Ia SNe redshift-luminosity (z-$L_{\rm app}$) relation. According to general relativity, this can only be caused by a dominant component of matter with a relativistically large negative pressure. Such matter, known as dark energy, is gravitationally repulsive, and not only causes the cosmological expansion rate to increase (the acceleration) but also causes a defocusing of light beams, making objects at a given distance appear smaller in angular size (demagnification), and thus in apparent luminosity (the z-$L_{\rm app}$ relation); or in other words "objects in this universe are closer than they *naively* appear". While the defocusing does not result in a shear of images it does have a number of effects on the shear which can be measured.

Quantitatively the demagnification by dark energy is the statement that the angular diameter distances, $D_{\rm A,co}(z_1, z_2)$ are increased. Since C_l depends on $D_{\rm A,co}(z_1, z_2)$ (see eq.s 14&15) what one measures from weak lensing will tell you something about the dark energy. The changes are quantitative and not qualitative. For example the $P(\frac{l}{D_{\rm A,co}(0,z)}, z)$ term means that different features in the 3d power spectrum will be moved around in l space, or in other words, will subtend a different angle as $D_{\rm A,co}(0, z)$ changes. By identifying features in the weak lensing power spectrum and seeing what angle they subtend one is performing the classical cosmological test of measuring a "standard rod", and by doing so one can infer the amount of demagnification, and hence the amount of

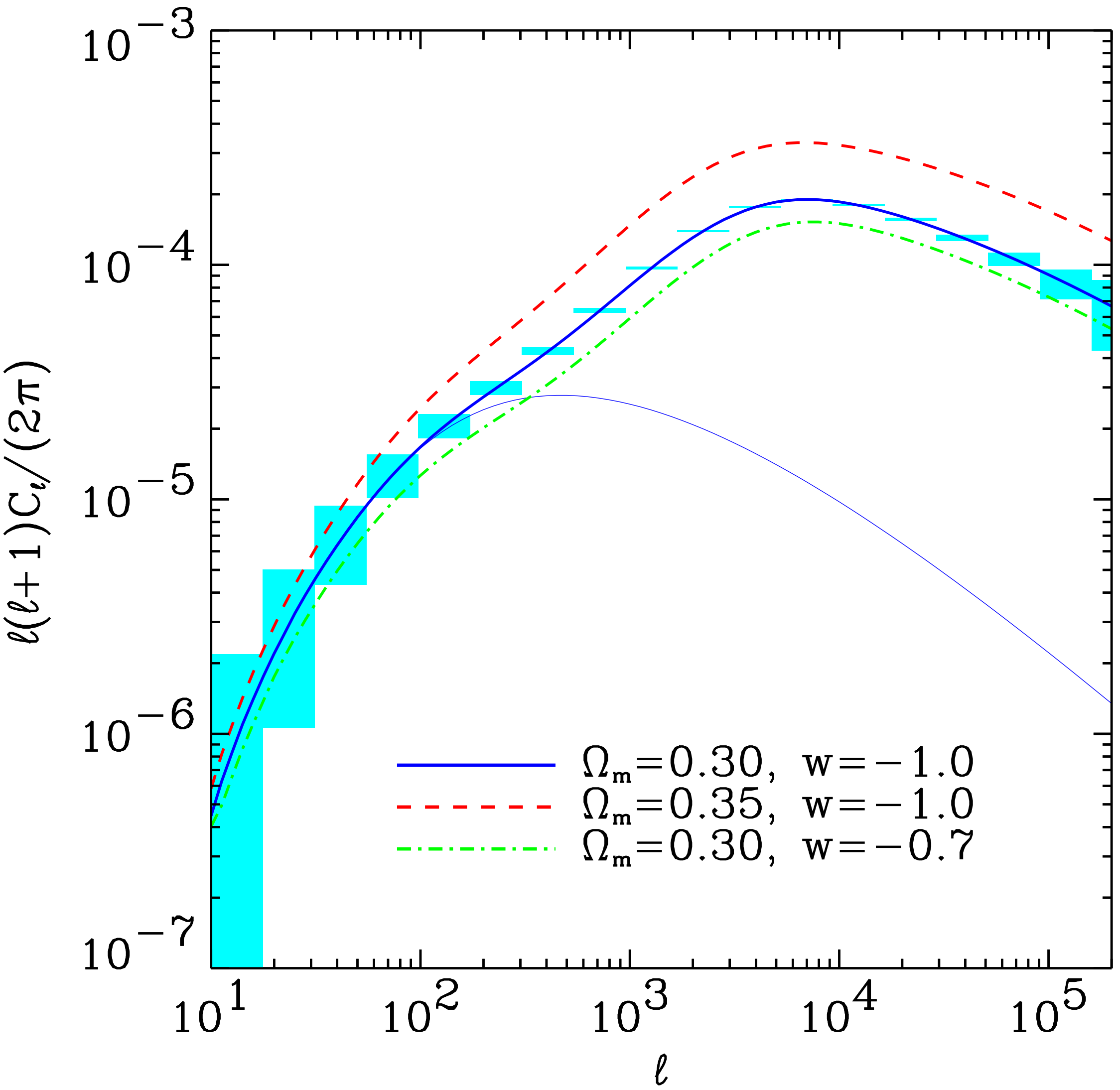

Fig. 11.— The shear angular power spectrum expect to be seen by the 300 square degree SNAP wide survey (taken from (Refregier et al. 2003b)). The dark blue, green, and red lines are predictions for different cosmological parameters as indicated; while the thin blue line is the prediction not allowing for nonlinear clustering of matter. The rectangles give the expected accuracy for the power in bands including both shape noise and sample variance.

negative pressure the dark energy exerts. Since the angular diameter distance is exactly what the SNe measure the two methods can be directly compared and provide a self check.

Another effect which does not come through the angular diameter distance is the growth factor, i.e. the z dependence in $P(k, z)$. This also depends on the dark energy which, since it is repulsive, suppresses growth of density inhomogeneities. Since we don't fully understand nonlinear growth of inhomogeneities it is possible that on nonlinear scales one cannot really disentangle theoretical uncertainties from the effects of dark energy. However on linear scales, which we see from fig 11 corresponds to $l \lesssim 200$, one will be able to probe dark energy using weak lensing. The Fermilab group which has strong research program in both weak lensing and nonlinear clustering should be able to optimize the analysis so as to avoid contaminating dark energy measurements with growth factor uncertainties.

4.2. Expected Accuracy and Survey Strategy

Since the main goal of the SNAP mission is to measure properties of the dark energy, it is essential to know how well a SNAP weak lensing survey can measure these same properties. Such a study has already been carried out in (Refregier et al. 2003b) obtaining results indicating that weak lensing approaches the accuracy of the SNe. They further conclude that an optimal strategy for a 5 month survey is gotten with an area ≈ 300 sq-degree. As noted elsewhere in this document both the time alloted and the area are smaller than what one might like for other projects probes of dark energy such as using cluster counts. Studies here at Fermilab question whether this (default) survey will really give the best handle on dark energy even from weak lensing.

The main issue is whether or not one can use the very large signal at small scales (see fig 11) to learn something about dark energy. We have argued that theoretical uncertainties in nonlinear clustering can be confused with the effects of dark energy. Most of the statistical leverage assumed by Refregier et al. (2003b) comes from $l \sim 10^4$ corresponding to comoving scales of $\sim 100\,\mathrm{kpc}$, which is highly nonlinear. In Refregier et al. (2003b) was voiced the hope that these theoretical uncertainties could be overcome by numerical modeling in the years prior SNAP's launch. We are less optimistic, that the required theoretical accuracy of $\lesssim 1\%$ can be achieved in a reliable way. In fact it seems equally plausible that weak lensing studies from a mission like SNAP will exceed in accuracy numerical modeling over the next decade. If we discount weak lensing information on the smallest scales because of theoretical uncertainties, and restrict ourself to linear scales, then quite a different picture emerges for the optimal SNAP weak lensing strategy as illustrated in fig 12. By limiting oneself to large (linear) angular scales where the shape-noise is small compared to the sample variance one is lead to increase the area (i.e. the sample) for greater statistical accuracy. This is in contrast to the case where one uses the smaller nonlinear scales where the signal-to-noise is small and shape noise dominates. In that case statistical accuracy leads one to make the survey deeper rather than wider in order to include more galaxies and thus reduce the shape noise. Of course this is not the whole story since systematic errors are also liable to be different on these different angular scales. The smaller signal at $l \sim 200$ leaves can be more susceptible to systematic errors in shape measurements than the relatively large signal at smaller angular scales.

4.3. Systematic Effects

This all sounds very good, but will it really work as advertised? The last section pointed out theoretical uncertainties in nonlinear clustering which can either be avoided by not using the small scale lensing data in extracting cosmological parameters, or theoretical progress in the time interval before or during the survey. There is also the uncertainty in the redshift distribution of galaxies which can be constrained by photo-z technique. (Huterer 2002) has shown that one does not need small photometric redshift errors in order to precisely measure the dark energy parameters, but one does need these errors to be accurately characterized. For example a systematic bias in z-estimators can lead directly into a systematic bias in w-estimators. People at Fermilab are studying this issue and it is expected that this will not be a significant source of error in determining dark energy parameters. People at Fermilab are also studying the first issue, but here we are less confident.

There are also instrumental effects. Let us first note that shear signal on angular scales $\lesssim 1^\circ$ (larger scales statistically contain very little cosmological information) is no smaller than has already been detected. SNAP should certainly detect weak lensing with very high significance. However in order to achieve the advertised sensitivity to cosmological parameters one requires that statistical shape noise remain the dominant error in the estimation of the shear. Sources of instrumental shear errors introduced by the SNAP telescope and detectors have been studied in detail in (Rhodes et al. 2003) who conclude that these all can be corrected for to sufficient accuracy if one monitors the image quality by periodic observations of stars and astrometric sources; and that the image quality and stability will exceed what can be obtained from ground based observations.

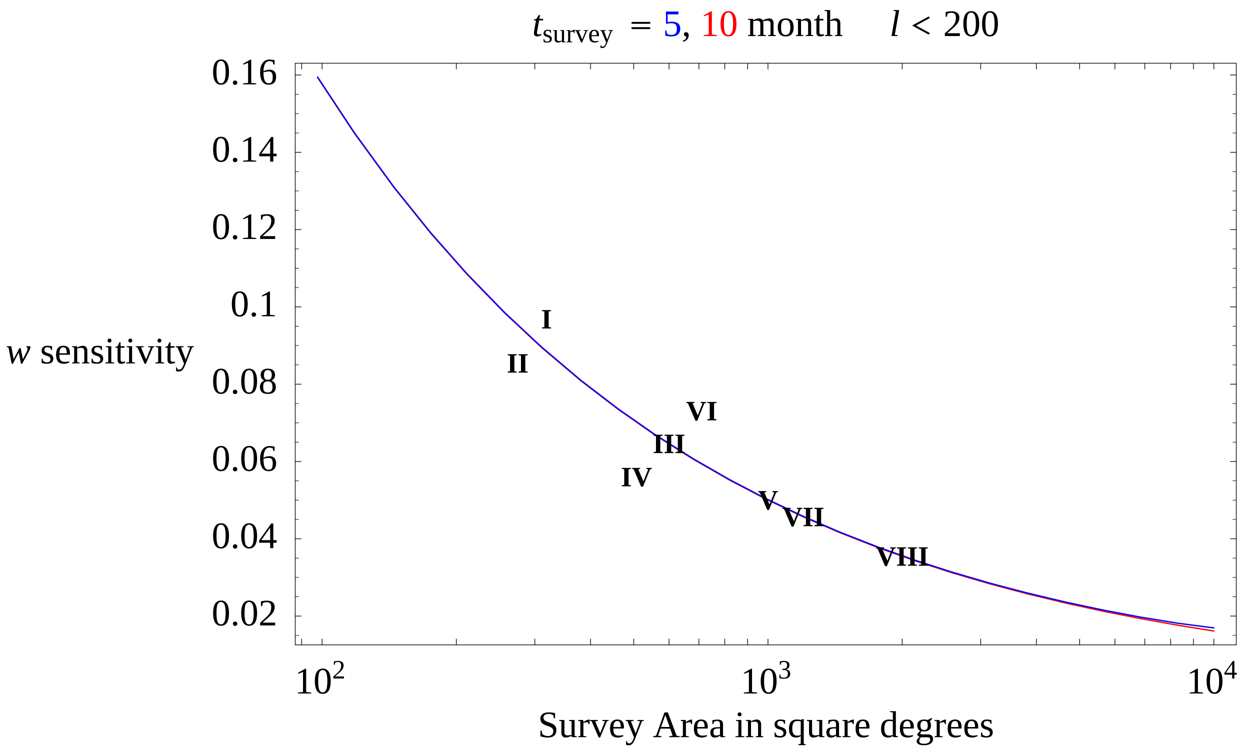

Fig. 12.— The sensitivity to the dark energy equation-of-state, w, for different survey strategies using only the linear, $l < 200$ weak lensing data. Specifically this is $F^{-1/2}$ where F is the Fisher information for w evaluated at $w = -1$, and degeneracy with other parameter may increase the w uncertainty. The red and blue lines are for a total survey time of 5 and 10 months, while the roman numerals indicate the survey parameters listed in table 2 (and have been offset slightly where they overlap). There is practically no dependence on depth but only on survey area, which points to a larger area survey for better dark energy accuracy.

5. Non-Dark Energy Science

As described above, SNAP will be a powerful instrument for constraining dark energy and related cosmological parameters, via supernovae, galaxy clusters, and weak gravitational lensing. However, separate from dark energy and cosmology, SNAP as a wide-field imaging survey telescope will also be an unprecedentedly powerful tool for studying populations of astronomical objects, particularly galaxies and quasars at high redshifts and faint magnitudes, as well as for constraining models for the formation and evolution of these objects. In this section we will describe a subset of such non-dark-energy science of particular interest to the Fermilab SNAP group, specifically the clustering properties of galaxies and and dark matter and the redshift evolution of galaxy populations.

5.1. Exploring the Clustering of Galaxies

The wide field survey capability of SNAP offers a unique opportunity to study galaxy clustering (in addition to mass clustering from weak lensing) and its evolution at high redshifts ($z \sim 0.3 - 3$). This is a regime that is particularly interesting for several reasons:

- Little is known about galaxy clustering beyond redshifts of 0.3 or so. There are some measurements of clustering at high z's from surveys with small fields, such as the Hubble Deep Field, and studies of Lyman-break galaxies at $z \sim 3$ (Steidel et al. 1996). Sample variance generally severely limits the accuracy with which the two-point correlation is measured from these surveys (Porciani & Giavalisco 2002). SNAP increases the size of previous high redshift surveys by several orders of magnitude.
- In a universe dominated by dark energy, structure grows slowly. Most of the large scale structure we see today grows at z larger than about 1, when the dark energy is a subdominant component of the total energy density of the universe. The $z > 1$ regime is therefore very interesting from the point of view of studying structure formation in action.
- From the point of view of constraining cosmological parameters, the $z > 1$ frontier is also interesting because one can probe the linear power spectrum down to smaller scales (down to $k \sim 1$ h/Mpc), because the nonlinear scale is smaller as one goes to higher redshifts. This is important in testing inflation, because to constrain the inflaton potential, one needs as long a lever arm as possible in the range of scales probed (Deustua et al. 2001).

A host of interesting cosmological constraints can be obtained from measurements of galaxy clustering, which will be elaborated below. But first, we need to introduce the statistics that quantify galaxy clustering, and discuss how one can relate this to the clustering of mass, which is generally more robustly predicted by theory.

Measurements of galaxy clustering– The most widely used, and useful, statistics is the two-point correlation function and its Fourier transform, the power spectrum (Peebles 1980):

$$\xi_2^g(r) = \langle \delta_g(x)\delta_g(x+r)\rangle \quad , \quad P^g(k) = \int d3r \xi_2^g(r) e^{-ik\cdot r} \tag{17}$$

where the galaxy fluctuation is $\delta_g \equiv (n_g - \bar{n}_g)/\bar{n}_g$, with n_g being the number density of galaxies, and $\bar{n}_g$ its mean.

Since the galaxy survey in question is a photometric one (no spectroscopic redshifts), the two-point function can be approached from 2 different directions.

One is to measure the galaxy clustering directly in 3 dimensional angle-redshift space, with the understanding that the error in the redshift direction is particularly large ($\Delta z \sim 0.1$). This creates what is not unlike very large scale finger-of-god redshift distortions. A simpler approach is to measure the angular correlation (2D analogs of eq. [17]) in coarse redshift bins of $\Delta z \sim 0.2$. Given the selection function, this can be inverted to obtain the 3D power spectrum.

Natural extensions of eq. 17 to higher number of points (three-point function, and so on) are very useful in constraining the nature of galaxy-biasing (i.e. the relation between galaxy distribution and mass distribution), a subject we will turn to next (Fry 1994, Scoccimarro et al. 2001).

Interpretations of galaxy clustering– The galaxy and mass distributions are generally related to each other in non-trivial ways, except on sufficiently large scales. We therefore focus here on the large scale clustering (above the nonlinear scale, which varies from $k \sim 1$ h/Mpc at $z \sim 3$, to $k \sim 0.1$ h/Mpc at $z \sim 0.2$).

On large scales, it is expected that the galaxy and mass fluctuations are related in a linear manner:

$$\delta_g(x) = b\delta_m(x) \tag{18}$$

where δ_m is the mass fluctuation, and b is commonly known as the galaxy bias, or bias for short. One can think of the above as the lowest order term in a systematic expansion in δ_m (Fry & Gaztanaga 1993). The higher order terms are important in discussions of higher order correlations, but we will ignore them for simplicity of presentation.

With the linear bias relation, it is clear that the galaxy power spectrum has the same shape as the mass power spectrum i.e. $\langle \delta_g(x_1)\delta_g(x_2)\rangle = b^2\langle \delta_m(x_1)\delta_m(x_2)\rangle$. In other words, at a minimum level, galaxy clustering tells us directly the shape of the mass power spectrum on scales above the nonlinear scale.

In fact, we can do better than that. Higher order clustering can be used to infer b. The idea works roughly as follows. The galaxy three-point correlation function is related to the mass three-point function by: $\langle \delta_g(x_1)\delta_g(x_2)\delta_g(x_3)\rangle = b^3\langle \delta_m(x_1)\delta_m(x_2)\delta_m(x_3)\rangle$. On the other hand, it is well known that gravitational instability, together with Gaussian initial conditions, predicts that the (mass) N-point function ξ_N is related to the (mass) two-point function ξ_2 by $\xi_N \sim \xi_2^{N-1}$, where the proportionality constant and configuration dependence can be worked out exactly using perturbation theory. This then implies that

$$\frac{\langle \delta_g(x_1)\delta_g(x_2)\delta_g(x_3)\rangle}{\langle \delta_g(x_1)\delta_g(x_2)\rangle\langle \delta_g(x_2)\delta_g(x_3)\rangle + \text{permutations}} \sim \frac{1}{b} \tag{19}$$

allowing us to measure the galaxy-bias directly. In reality, the above expression is modified by the higher order terms ignored in the linear bias relation (eq. [18]). They, however, do not change the fundamental conclusion that one can use the higher order correlation functions to measure the galaxy-bias.

Cosmology from galaxy clustering– There are a host of interesting cosmological constraints that will come from measurements of galaxy clustering from the SNAP wide field survey.

1. Measurements of the galaxy power spectrum shape as a function of redshift allows us to infer the evolution of the Hubble parameter. Specifically, features in the galaxy power spectrum, such as its peak, provide a standard yardstick for measuring angular diameter distances, much like what supernova do.

2. Using higher order statistics as outlined in the last section, one can obtain the bias of the galaxy power spectrum, hence allowing us to infer both the amplitude and shape of the mass power spectrum on large scales. In conjunction with probes such as the microwave background, galaxy clustering then allows us to measure the primordial spectral index over 3 orders of magnitude in scale. This is important in constraining the possible running of the spectral index, and the presence of tensor modes (which contribute to the microwave background but not to the galaxy clustering signal).

3. The gravitational lensing mass power spectrum together with the galaxy power spectrum can be used to constrain the galaxy-bias (independent of arguments making use of higher order correlations). The scaling of the N-point function with the two-point function, as in eq. (19), can then be used to constrain non-Gaussianity in the initial conditions.

4. An interesting use of the SNAP wide field survey is to cross-correlate the galaxy distribution with the microwave background. Expected sources of cross-correlation include Sunyaev-Zeldovich distortions as well as the integrated Sachs-Wolfe effect. The former tells us about the nature of hot gas around galaxies , while the latter provides a probe of dark energy.

It should be noted that several of the above cosmological constraints can be obtained from the lensing mass power spectrum as well. Since the galaxy clustering information is there, there is no reason not to use it in addition to the weak lensing signal to increase the scientific return and decrease error-bars on cosmological parameters.

5.2. Galaxy Evolution

The population of galaxies in the universe is comprised of a diverse mix of objects of different luminosities, spectral properties, colors, shapes, and sizes. The details of the formation and evolution of galaxies and of their constituent stars are likewise often complicated and not well understood, particularly at high redshifts. A large number of imaging and spectroscopic surveys have been carried out to study galaxy populations and their evolution, but it is important to emphasize that the SNAP Wide Area Survey will constitute an unprecedented and unique galaxy sample.

Advantages of SNAP– Essentially, SNAP is unique because of its unprecedented combination of large survey area and sample size, broad wavelength coverage, imaging and redshift depth, and high spatial resolution. The fiducial 1000 deg^2 Wide Area Survey is nearly 10^6 times larger than the 5 arcmin^2 area covered by the Hubble Deep Field (HDF) North (Williams et al. 1996), which has revolutionized galaxy evolution science despite its small size. Moreover, the Wide Area Survey imaging depth is only modestly shallower ($\sim$ 1 mag) than that of HDF, and SNAP also has more optical filters (6 vs. 4) plus an additional 3 near-IR filters. The SNAP area and size are also very significant advantages compared to planned Hubble Space Telescope surveys of similar imaging depth, most notably GOODS, which will cover only 320 arcmin^2. Likewise, though ground-based surveys like LSST will cover more sky ($\sim 10^4$ deg^2), SNAP provides the important dual advantages of being in space: (1) deep near-IR photometry, which permits unbiased sampling of important galaxy populations at high redshifts $z \gtrsim 1$; and (2) high spatial resolution, which allows detailed structural and morphological measurements of high-redshift galaxies otherwise not possible below the atmosphere. Finally, a number of ground-based spectroscopic redshift surveys (VIRMOS, DEEP) on large 8-10m class telescopes will gather substantial galaxy redshift samples ($\sim 10^5$ objects) at $z \lesssim 5$, but the depths for the bulk of such samples are several magnitudes shallower than that of SNAP and the sky coverage is < 20 deg^2. In contrast, the fiducial 1000 deg^2 Wide Area Survey will gather about 3×10^8 objects to deeper limits ($I_{AB} < 26.2$), with photometric redshifts of sufficient accuracy for most galaxy evolution and galaxy clustering applications. In short, the SNAP Wide Area Survey will provide a combination of area, size, depth, and wavelength coverage that is unmatched by other samples, either space- or ground-based, for galaxy science studies.

Luminosity Functions and Galaxy Populations– The luminosity function (LF) simply gives the galaxy number density as a function of galaxy intrinsic luminosity; it is a basic but fundamentally important statistic for the characterization of galaxy populations and their evolution. Galaxy luminosity functions have been measured in the local universe ($z \sim 0.1$) from many different redshift surveys, including very large recent samples ($> 10^5$ galaxies) from the 2dF (Nordberg et al. 2002) and SDSS (Blanton et al. 2003). Likewise, the evolution of the galaxy LF has been probed using deeper but much smaller samples (typically $\sim 10^3$ galaxies), out to redshifts $z \sim 4$ (e.g., Lilly et al. 1995; Ellis et al. 1996; Lin et al. 1999; Steidel et al. 1999). The LFs of different galaxy populations are known to differ systematically, depending on galaxy properties such as spectral type, color, and morphology. Likewise, the evolution of the luminosity function is observed to depend on galaxy properties, with strong evolution seen for blue, late-type, star-forming galaxies, contrasted with modest changes observed for red, early-type, more quiescent objects.

However, existing galaxy samples at intermediate to high redshifts ($z \sim 0.3 - 5$) are generally far from large enough to constrain, in *detailed quantitative* terms, the LF evolution of different galaxy populations, even for simple parameterizations of luminosity and density evolution in the LF (Lin et al. 1999). Also, the redshift range $z \sim 1 - 2.5$ is not as well surveyed as the $z < 1$ or even the $z \sim 3 - 4$ regime, due to the difficulty of the required near-IR observations when carried out from the ground. Moreover, because of the optical selection technique used, at high redshifts $z \gtrsim 2$ one samples primarily strongly star-forming objects, the so called Lyman-break galaxies (LBGs), and one may be missing a substantial population of more normal galaxies which require near-IR selection (recently found by van Dokkum et al. 2003). Ideally, one would prefer a galaxy LF sample akin to what the SDSS provides for the local universe, i.e., a sample consisting of a large number of galaxies (10^6 or more) with detailed multi-band photometry and well-understood sample selection effects. The SNAP Wide Area Survey indeed provides this: 3×10^8 galaxies for the fiducial 1000 deg^2 survey ($I_{AB} < 26.2$), with well-calibrated 9-filter optical plus near-IR photometry that allows unbiased galaxy selection to $z \approx 3$, and selection of Lyman-break galaxies to higher redshifts. Although there is generally no spectroscopic redshift data for Wide Area Survey galaxies, for the LF and other statistics described below, photometric redshifts will provide both necessary and sufficient redshift information (uncertainties $\sigma_z \sim 0.05 - 0.2$; see §9.1). The SNAP Wide Area Survey should therefore provide thorough and definitive measurements of the evolution of the luminosity function and other statistics for a broad range of galaxy populations at intermediate to high redshifts. Fermilab SNAP scientists will use this exceptional data set to constrain models of the evolution of galaxy populations, as we outline next.

Galaxy Evolution Models and Star Formation Histories– The evolution of the spectral energy distribution (SED) of a galaxy may be modeled, given some prescription for the time dependence of the star formation rate (SFR) within that galaxy. For example, an elliptical galaxy may be modeled under the simple assumption that all its stars formed solely in an initial, δ-function-like burst of star formation. In contrast, spiral and irregular galaxies do have ongoing star formation, and these galaxies need to be modeled with more continuous star formation histories. Once such an SFR history is specified, the galaxy's SED evolution may then be predicted, using well-understood stellar evolution theory, from the luminosity and spectral evolution of the specified population of stars which comprise that galaxy.

The 9-band optical and near-IR photometry in the SNAP Wide Area Survey then provides the data needed to constrain such galaxy evolution models and star-formation histories. In particular, SNAP's broad wavelength coverage samples the full range from the rest-frame ultraviolet, dominated by younger stellar populations (as in star-forming galaxies), to the rest-frame optical/near-IR, dominated by older stellar populations (as in elliptical galaxies). See Figure 13 for some examples of SED model fits to high-redshift galaxies which have both optical and near-IR photometric data. Furthermore, because of SNAP's high spatial resolution, it will be possible to measure the SED as a function of position *within* a particular galaxy, and thus to identify separate intra-galactic stellar populations with different formation histories. Such detailed studies have been carried out only for a small handful of high-redshift galaxies from Hubble Space Telescope observations, but again, SNAP will do so systematically for an orders of magnitude larger data set.

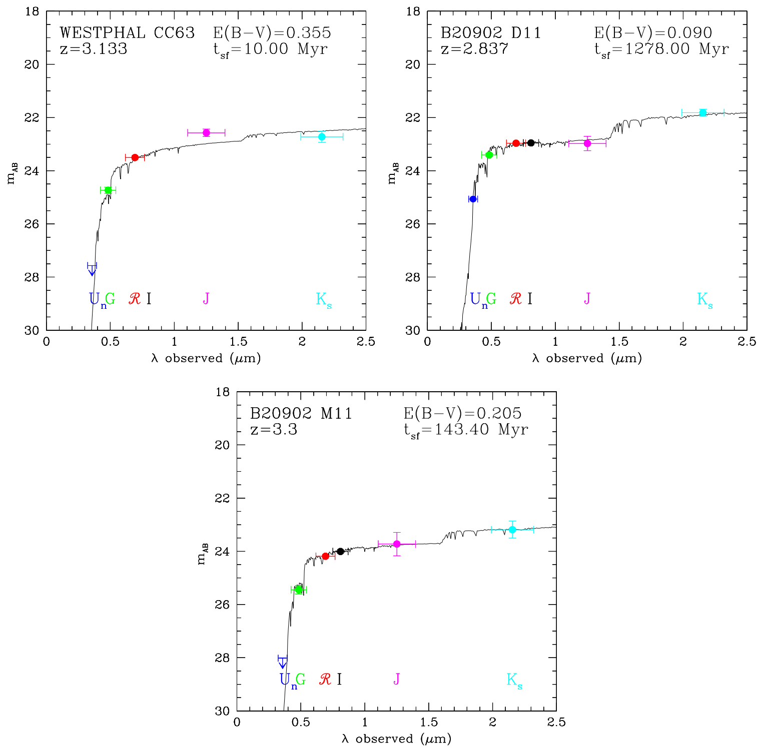

Fig. 13.— Examples of fits of galaxy spectral energy distribution models to three high-redshift galaxies with both optical and near-IR photometric data. (Shapley et al. 2001)

Quantitative Galaxy Morphology– Historically, galaxy morphologies have been classified using the Hubble sequence, with elliptical, spiral, and irregular galaxy types. However, such classifications are usually done by eye and therefore are subject to human bias, and they are also impractical to carry out for very large samples. Moreover, the Hubble Deep Field (HDF) and other samples have shown that at high redshifts, increasing fractions of galaxies are no longer adequately described by Hubble type classifications. A number of quantitative morphology statistics have therefore been developed to address these issues, such as measures of the concentration and asymmetry (e.g., Abraham et al. 1996; Bershady et al. 2000) of the 2D galaxy light profile, and fitting techniques which decompose galaxy profiles into disk and bulge components (e.g., Schade et al. 1999; Simard et al. 2002). Possibly most interesting is the decomposition of galaxy profiles into a set of 2D basis functions known as "shapelets" (e.g., Refregier et al. 2003a). This technique has already been used for generating galaxy image simulations for SNAP weak lensing science trade studies (Massey et al. 2003b). The shapelet formalism provides a convenient quantitative means for describing not only the traditional Hubble galaxy types, but also the often complex morphologies of high-redshift galaxies, which may be characterized by irregular shapes with complicated knots of star-forming regions. See Figure 14 for an illustration of the use of shapelets to model HDF galaxies.

Again, the SNAP Wide Area Survey provides an unprecedented sample for quantitative galaxy morphology studies, most importantly in terms of the high spatial resolution (SNAP point spread function FWHM = $0.15''$) required to accurately measure the sizes and morphologies of the often small objects which comprise the high-redshift galaxy population. SNAP will therefore permit definitive measurements of the evolution of the joint distributions of morphologies with other properties such as luminosities and SED types. These quantitative morphology studies will serve as a natural nexus for the Fermilab SNAP group's strong interests in the galaxy shape measurements needed for weak lensing and in the statistics of evolving galaxy populations.

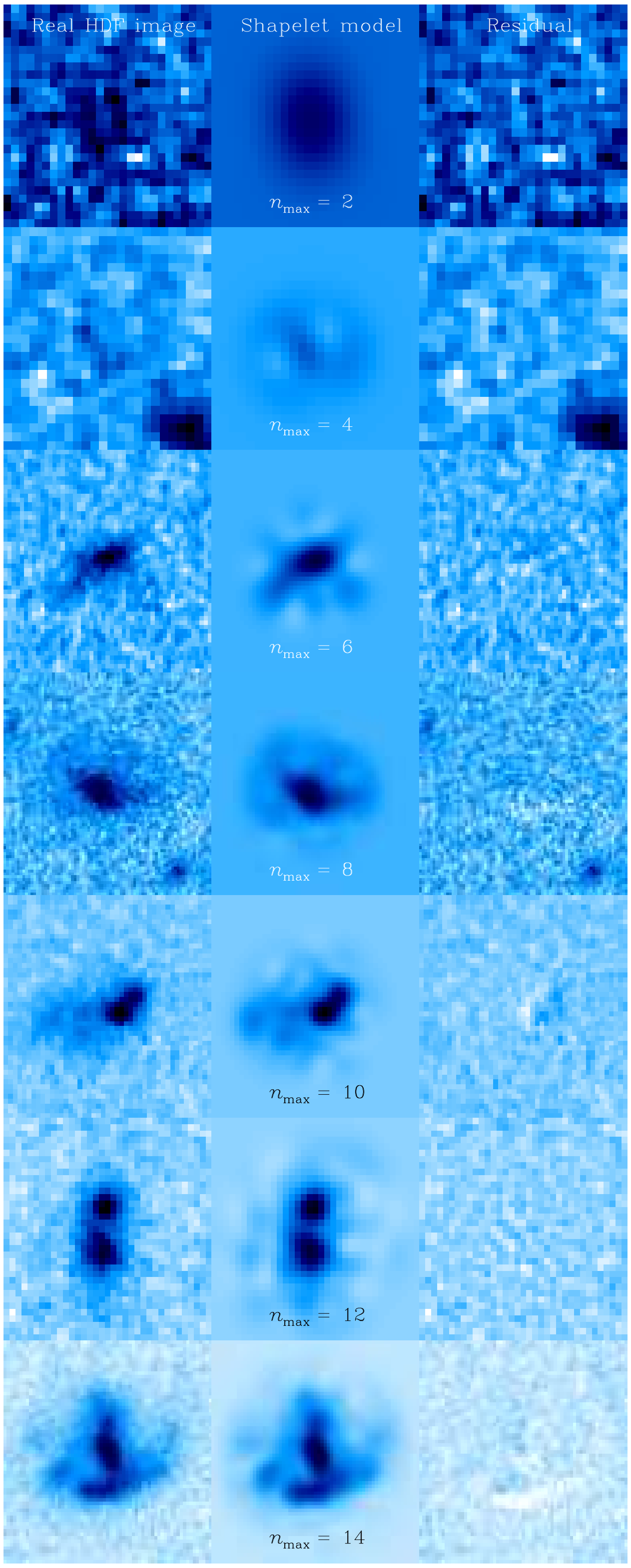

Fig. 14.— Shapelet modeling of a selection of HDF I-band galaxies. Higher S/N galaxies typically require more shapelet coefficients and we display a variety of source galaxies, noting the number of shapelet coefficients $n_{\rm max}$ required to reach a reconstruction with reduced $\chi^2_r = 1 \pm 1\sigma$. In all cases, the first column shows the original HDF image; the middle column shows the shapelet model; the right column shows the residual. The image size and color scale is different for each row. (Massey et al. 2003a)

6. Fermilab Contributions to the Experiment

There are three methods to investigate dark energy that appear to be most effective when studied from SNAP—supernovae as standard candles, weak lensing measurements of the matter power spectrum, and cluster counting to measure cluster evolution. Fermilab scientists believe that the SNAP mission can be made stronger if the proposed wide area survey portion of the mission is enlarged from 300 to about 1000 square degrees. This will, of course, make the weak lensing result better, but equally important, it will open up cluster counting as an effective way to study dark energy. Fermilab scientists are interested in all three methods, but are particularly involved in using large-scale structures as a dark energy probe. We propose that the SNAP@Fermilab group accept responsibility for the SNAP wide area survey. We have not emphasized the fact that such a survey would be an extremely valuable legacy for astronomy, but this remains a very interesting aspect to SNAP's astronomical collaborators, including NASA.

The SNAP@Fermilab group has in the past year been working towards making an overall plan for contributing to SNAP and gaining admission into the international SNAP collaboration. The Fermilab group, initially comprising about 30 scientists from all four divisions, submitted a letter requesting admission into the SNAP collaboration outlining work that Fermilab proposes to accomplish. In addition, a component of our group was involved in investigating the possibilities of ground or space-based experiments to commence earlier than SNAP, in order to fill the next few years with a science-based program.

We have developed a proposed Fermilab work list. In order to be on the Fermilab work list, the proposed work had to satisfy the following criteria:

- The work must be useful to SNAP and the SNAP collaboration.
- Fermilab should have special expertise in the required scientific skills and or technology, or the work scope should require national laboratory capability.
- Preference was given to work that supports science of particular interest to the Fermilab collaborators.

The proposed scope of work falls into three broad categories in addition to Fermilab's science efforts, which involve extensive investigation of the science and performance of the mission through calculations and simulations.

- Software Design– The data from SNAP must be put into a form that is useful to the collaboration and the public. Fermilab has expertise in this field due to its involvement in SDSS. We expect that most of this work will involve the wide-field survey.

- Hardware Design– Fermilab's proposal to enlarge the wide-field survey may affect some aspects of the mission, in particular, creating a larger data set. Fermilab proposes to work on electronics that will help mediate those issues. We are exploring a solid state recorder to store more data on board, and improved data compression hardware to reduce the size of the stored data set for the wide area survey.

- Science Support– Science algorithms made concrete in code that are necessary for the success of the science mission but are not directly in the analysis path. Our two examples are photometric redshifts and cluster finding algorithms, but also includes the photometric calibration. SNAP requires better calibration that any previous survey. Fermilab has particular expertise due to its involvement in SDSS.

The following sections describe these contributions in more detail.

7. Software Design

7.1. Wide Area Survey Data Pipeline and Data Factory

The Fermilab Experimental Astrophysics group has spearheaded Sloan Digital Sky Survey (SDSS) data processing and operations for over a decade. The Experimental Astrophysics Group operates the data processing factories; developed and maintains several of the science pipelines; provides overall coordination of the science (and infrastructure) software; distributes data to the collaboration for scientific analyses; prepares, operates, and supports public data releases, including documentation and help desks. We propose to perform similar work for the Supernova Acceleration Probe (SNAP).

Our capabilities for this work are high: As of Jan 2003 we spin 35 terabytes for data processing and data distribution. We manage the running of upwards of 10 scientifically interesting pipelines on the SDSS data, and different databases for operations and data distribution. We run these pipelines on the compute farms Fermilab, early models for the beo-clusters of the grid; and are nearly always working in the realm where the prime bottleneck for processing is human debug cycles despite the high data throughput. We use the Fermilab Enstore mass storage system extensively, a model for future data storage grids. We are working in NVO and Grid collaborations both inside and outside Fermilab. We are at the forefront of data and compute intensive astrophysical surveys.

The majority of the SNAP@Fermilab's research interests in SNAP – probes of cosmology via weak lensing and clusters of galaxies – are best addressed with the Wide Angle Survey. We thus would propose to hand the data processing and distribution for the WAS, as they resemble SDSS imaging processing, and the effort required to do the SNAP WAS data processing and distribution is similar to that required for the SDSS.

In particular, we would imagine working on the image processing pipelines.

Corrected Frames– The images produced by the camera must have the instrumental signatures removed. This includes bias, flat field, and cosmic ray rejection. What is left are images that could in principle be used for science, what the SDSS knows as corrected frames.

Final Images– Given the photometric calibrations (which SNAP@Fermilab will contribute to) and the astrometric calibrations, the multiple images that cover the same part of the sky must be added together in an optimal way. The resulting images are the final images, ready for science.

Catalogs– The images are then ready for object detection, classification, and measurement. These are some of the most scientifically interesting aspects of the image processing. We have experience withe the relevant questions and problems from our SDSS work, and we would imagine adopting and modifying the most successful of the algorithms and ideas of the SDSS Photo pipeline in a new galaxy measurement code. The output of these are catalogs of every star and galaxy detectable in the final images.

Flat file data access– Many or all of the intermediate data products leading to the catalog are of interest to science collaborators. We would make organized data archives for all of the flat file products (final images and catalogs for each field are the prime examples), ensure they have backups, and allow for efficient data distribution and replication. As we imagine that there would be several sites that develop specialized pipelines for specific science problems and that these sites would all wish access to the final images, this is an important task.

Database data access– For many science questions databases may be constructed that allow for efficient, nearly optimal access to the data. We will provide databases optimized for the cluster counting and weak lensing problems we are most interested in: these will be widely useful beyond this narrow motivation.

Factory work– Factory work is necessary for survey production. Data providence and the ability to recreate data at will are crucial for large scale surveys. We will create 3^{rd} generation factory software to orchestrate processing of data streams, monitor progress, and report on data, software, and compute hardware defects.

Software collaboratory– We have experience with large distributed science software projects. We will install the discipline of data models and the documentation of final and intermediate data products in such a data model. We will install the discipline of collaborative tools for software development and maintenance: tools for SNAP that CVS and UPS played for the SDSS. We can provide bug tracking and listserve mailing lists. We will provide access for collaborators interested in the WAS data to review science code and work with us to add features that will enable their research.

8. Hardware Design

The Fermilab SNAP group has begun to contribute on hardware projects for SNAP. In selecting items to work on, the group has focused on projects that are important to the overall SNAP mission, utilize existing Fermilab expertise or are of a scope that require the infrastructure found at Fermilab, and are relevant for the base and expanded science interests. The Fermilab SNAP group has focused on two areas of hardware contribution: electronics and the radiation shield.

8.1. Electronics

In the area of electronics, the Fermilab group has begun R&D associated with components necessary for creating a data set expanded by a wide area survey. In particular, work has begun on the solid state recorder (SSR) and the data manager that is responsible for data compression.

Solid State Recorder– The SNAP solid state recorder consists of devices that store the imaging and spectroscopic data prior to transmission to the ground observing station. A solid state option is preferred since it would consist of no moving parts that would otherwise need to be compensated for by spacecraft control. The scope of the SSR is large even with the supernovae mission alone. In the current plans, approximately 85% of the three day orbit would be utilized for acquiring data from the optical and infrared cameras. Both the photometric and spectroscopic data from this three day orbit would require approximately 3 Tbits of storage after compression. For the wide area survey, it is thought the storage capacity may need to be a factor of two larger since many more images will be acquired (less spectroscopic observing). It is noted that 5.4 Tbits is the amount of data that can be transmitted using telemetry at 300 Mbs for 5 hours.

The initial thinking is that a space-qualified vendor would actually produce the SSR. Fermilab, however, would be responsible for various tasks associated with the procurement of the SSR. These tasks include making technology decisions, writing specifications, carrying out the procurement plan, and performing tests and measurements on preproduction and production components. In FY03, a modest R&D program has begun towards these efforts. Specifically, we are investigating whether state-of-the-art FLASH memory chips would be a viable technology on which to base the SSR. The key advantage to this technology is that the power requirements are estimated to be 1/10 the power of a similar system based upon DRAM devices. The major open issue is the radiation tolerance of FLASH memories in space environments. The R&D to be carried out includes the procurement of FLASH devices, mounting them on a custom printed circuit board, operating and evaluating the devices before and after exposure to a radiation beam. This effort builds upon similar studies of other integrated circuits and expands the Fermilab knowledge base by focusing on devices produced with feature sizes smaller than those used in the current generation of custom produced integrated circuits.

Data Manager– The data manager is a system of electronics that interfaces various pieces of onboard electronics with the solid state recorder and the telemetry systems. A core function of the data manager is to compress the image data so that more data can be appropriately stored. The data manager also exists as a critical component of the entire spacecraft electronics' system architecture.

The FY03 modest R&D program associated with the data manager includes evaluating different data compression algorithms by conducting a literature search and performing simulations on candidate algorithms. The data compression algorithms have both a software and hardware component. The software component includes the programming to implement the algorithm while the hardware component includes the implementation into suitable space qualified electronic circuitry. On the software side, it is anticipated that the supernova program will acquire data that is compressed using a lossless algorithm such as the Rice algorithm that has been used on NASA missions. For the wide survey, it is anticipated that a greater data compression factor will be required and several different schemes will be investigated. The data manager also will encode error detection and correction bits into the data stream so that a small number of bit errors can be fully recovered.

On the hardware side, much of the algorithmic encoding is planned to be done in a space qualified field programmable gate array chip (FPGA). It is planned that an FPGA evaluation printed circuit board be designed and used for data compression studies on image data relevant for SNAP. In addition, the printed circuit board can be used for examine FPGA behavior upon exposure to radiation during testing that overlaps with the SSR R&D described above. The data manager R&D includes proposing and developing system architecture considerations in coordination with the overall SNAP electronics plan. Like the SSR, the end deliverable of the R&D phase will be the contribution into the conceptual design report including technology recommendations and procurement plan with cost and schedule estimates.

Other electronics contributions– Fermilab also has specialized resources in the area of electronics that may prove to be valuable to the success of the SNAP project. In particular, the ASIC group within the electronics engineering department may be called upon to design custom circuitry associated with the control and monitoring of the focal plane and infrared detectors. In a similar manner, Fermilab has expertise in microwave radiation that might be beneficial in the specification of the data telemetry systems, and expertise in the assembly of large silicon detectors that might be beneficial for the assembly of the focal plane. Contributions into these areas could begin after SNAP is fully approved as a Fermilab project.

8.2. Radiation Shield

The current design for radiation shielding on SNAP includes several components which mush be designed and integrated into the spacecraft. The thermal shield and radiator is used to maintain stable operating temperatures especially for the instruments of the focal plane and the electronics. The focal plane cosmic ray shield is used to reduce the cosmic ray background during image exposures on the CCD's and infrared detectors. This cosmic ray shield also functions to lower the radiation exposure to the focal plane and electronics due to cosmic rays, the solar wind, and Van Allen belt radiation. The spectrograph cosmic ray shield has a similar function to protect the spectrograph and may include the passive radiator. Fermilab has positioned itself to take a leadership role and have responsibility for the cosmic ray shielding and will contribute to the design and possibly the fabrication of other components necessary to integrate these shields.

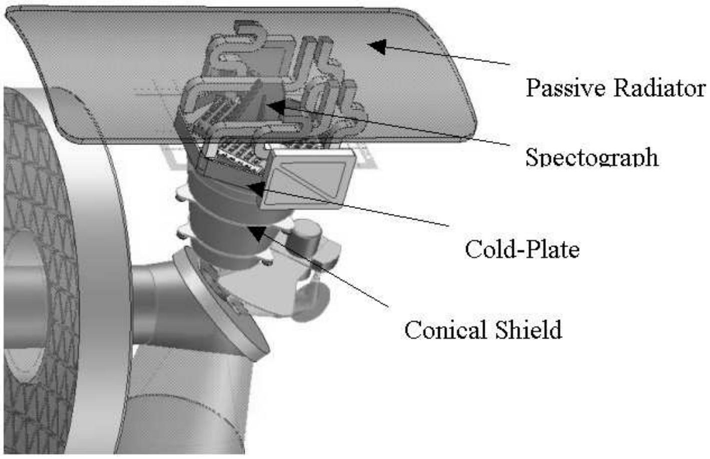

Fig. 15.— The cosmic ray shield in the current design of the SNAP instrumentation as the gray-colored object underneath the octagonal cold-plate on which the imaging detectors are mounted.

Cosmic Ray Shield– The cosmic ray shield in the current design of the SNAP instrumentation section is a conical-shaped metallic piece approximately .6 m in length and .3 m in radius at the base. It is shown in the figure Fig. 15 as the gray-colored object underneath the octagonal cold-plate on which the imaging detectors are mounted. In this location, the cosmic ray shield not only protects the sensors and electronics from radiation but also functions to thermally isolate the cold-plate from warm thermal sources and to reflect or absorb stray light. Fermilab's efforts on the cosmic ray shield utilize engineering resources within the Fermilab Technical Division supported by physicists from the Beams and Particle Physics Divisions.

The physics design of the cosmic ray shield involves understanding the cosmic ray and other radiation exposure expected by the SNAP spacecraft. Simulation and modeling of this radiation using the GEANT and MARS software packages will allow for estimating the radiation effects on the detectors and electronics and how appropriate design of the shield can mitigate these effects. The design of the shield will also have to take into other constraints such as the mass budget allowed for various spacecraft components. The engineering design must take into account the physics design and optimize the cosmic ray shield for mechanical characteristics such as stability, thermal properties, integration into other mechanical structures of the spacecraft, cost, etc.

The goal of the initial work on the cosmic ray shield will be to make an accurate estimate of the resource requirements during the SNAP R&D, design, validation, and fabrication phases. This work has started and will continue with participation in the writing of the conceptual design report. Engineering work will include both the thermal and structural analytical modeling of the shield, its supports, and interaction with the optical bench. Work will also include identifying a space chamber or procuring such a chamber for vacuum and thermal testing of the shield and mock-ups. The cosmic ray shield and other related components on board the SNAP spacecraft have critical function that can be accomplished only with detailed physics understanding and the associated engineering work.

9. Science Support

Science support is science algorithms made concrete in code that are necessary for the success of the science mission but are not directly in the analysis path.

9.1. Photometric Redshifts

In the absence of spectroscopic data, the redshifts of galaxies and other extragalactic objects may be estimated using solely multi-band photometric data, which may be thought of as very low resolution spectra. Though such "photometric redshifts" are necessarily much less accurate than true spectroscopic redshifts, they nonetheless can provide reliable redshift estimates that are sufficient for a large variety of science applications, with the advantage that photometric redshifts may be obtained more inexpensively and for much larger samples than is possible with true spectroscopy. In particular, photometric redshifts provide essential data for carrying out the various science goals of the Wide Area Survey, as spectroscopic redshifts will otherwise not be obtained by SNAP for Wide Area Survey objects.

There are two major approaches to measuring galaxy photometric redshifts. The first relies on fitting model galaxy spectral energy distributions (SEDs) to the photometric data, where the models span some range of expected galaxy redshifts and spectral types (e.g., Sawicki et al. 1997). The second approach depends on using an existing spectroscopic redshift sample as a training set to derive an empirical photometric redshift fitting relation (Connolly et al. 1995). There are advantages and disadvantages in either approach, as well as a number of variants and hybrids of these basic techniques (e.g., Csabai et al. 2003). However, photometric redshift methods ultimately rely on measuring the signal in the photometric data arising from prominent "break" features present in galaxy spectra, e.g., the 4000Å break in early-type galaxies, or the Lyman break at 912Å in star-forming galaxies. The key is to have photometric bands which straddle such break features throughout the redshift range of interest, so that the primary redshift signal may be readily detected. Additional refinements in the photometric redshift measurement then come from the strength of the break features and the gross shape of the galaxy SED, as determined by the photometric data on either side of the spectral break.

Clearly, in order to measure accurate photometric redshifts, it is important to have an adequate number of photometric filters with the appropriate wavelength coverage. At redshifts $z < 1$, a photometric redshift uncertainty $\sigma_z \sim 0.05$ (e.g., Csabai et al. 2003) may be readily achieved using 4-5 broadband optical filters covering approximately 3000-9000Å (e.g., with the "UBVRI" or SDSS "ugriz" filter sets), with S/N ~ 10 in each filter. At $z \sim 1-3$, near-IR imaging (typically 0.9-2.2 μm) is necessary to obtain good photometric redshifts, since the 4000Å break has now redshifted to wavelengths $\gtrsim 1\mu$m. For redshifts $z \gtrsim 3$, optical imaging alone allows detection of the Lyman break of star-forming galaxies and provides photometric redshifts with $\sigma_z \sim 0.2-0.3$ (e.g., Lanzetta et al. 1996; Sawicki et al. 1997). Moreover, the addition of near-IR data to the optical imaging

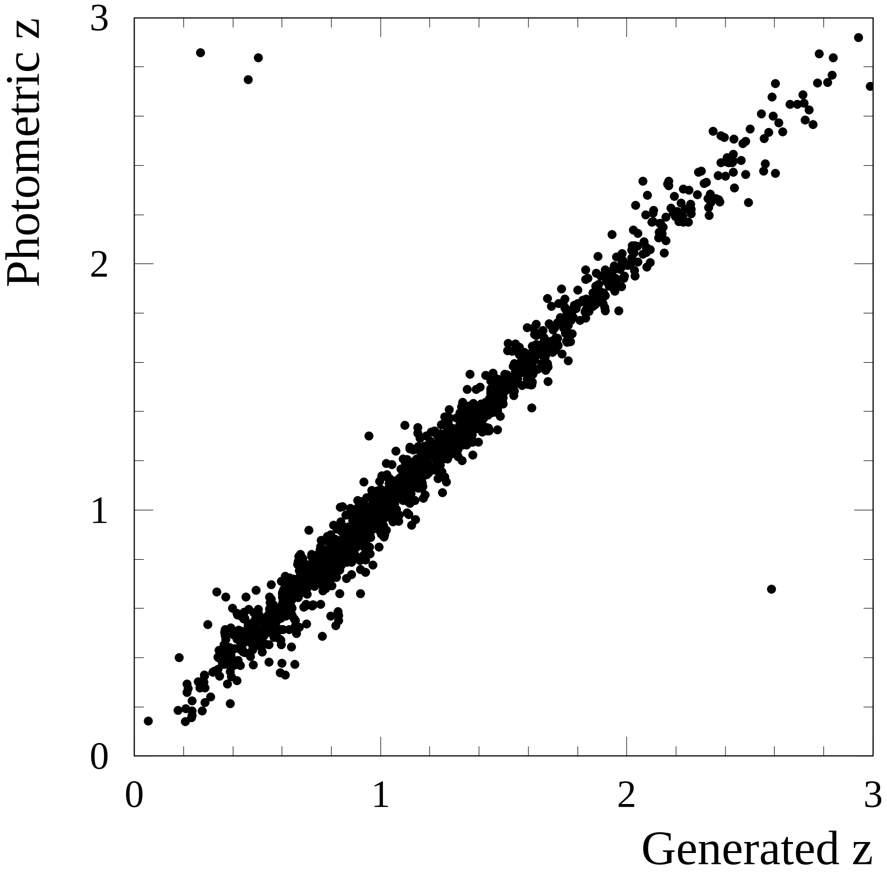

Fig. 16.— Generated redshift vs. reconstructed photometric redshift for a simulated population of galaxies as expected from the wide-angle survey. From Ref. Massey et al. (2003b).

at these high redshifts $z \gtrsim 2-3$ further reduces photometric redshift uncertainties down to the $\sigma_z \sim 0.1-0.2$ level (Massey et al. 2003b; Vanzella et al. 2002), and also permits detection of the 4000Å break for non-star-forming objects. Thus SNAP, with its full complement of 6 optical and 3 near-IR filters (covering about 3500-17000Å), will provide accurate photometric redshifts out to at least $z \sim 5-6$, currently the upper limit for galaxies with known spectroscopic redshifts. See Figure 16 for a simulation of photometric redshifts for the SNAP Wide Area Survey.

In the case of our design matrix rows VI, VII, and VIII we explore surveys using only 3 optical filters. As long as the 3 filters span the wavelength of the 4000Å break at the required redshifts, we expect accuracy to be maintained but that precision will be somewhat reduced. This is an area of current research.

Also, the reliability of any photometric redshift galaxy sample ultimately hinges on verification using spectroscopic redshifts for some representative subset of the sample. Though SNAP will not obtain spectroscopic redshifts for the Wide Area Survey, the SNAP Supernova Survey will provide about 2000 spectroscopic redshifts that may be used for photometric redshift verification

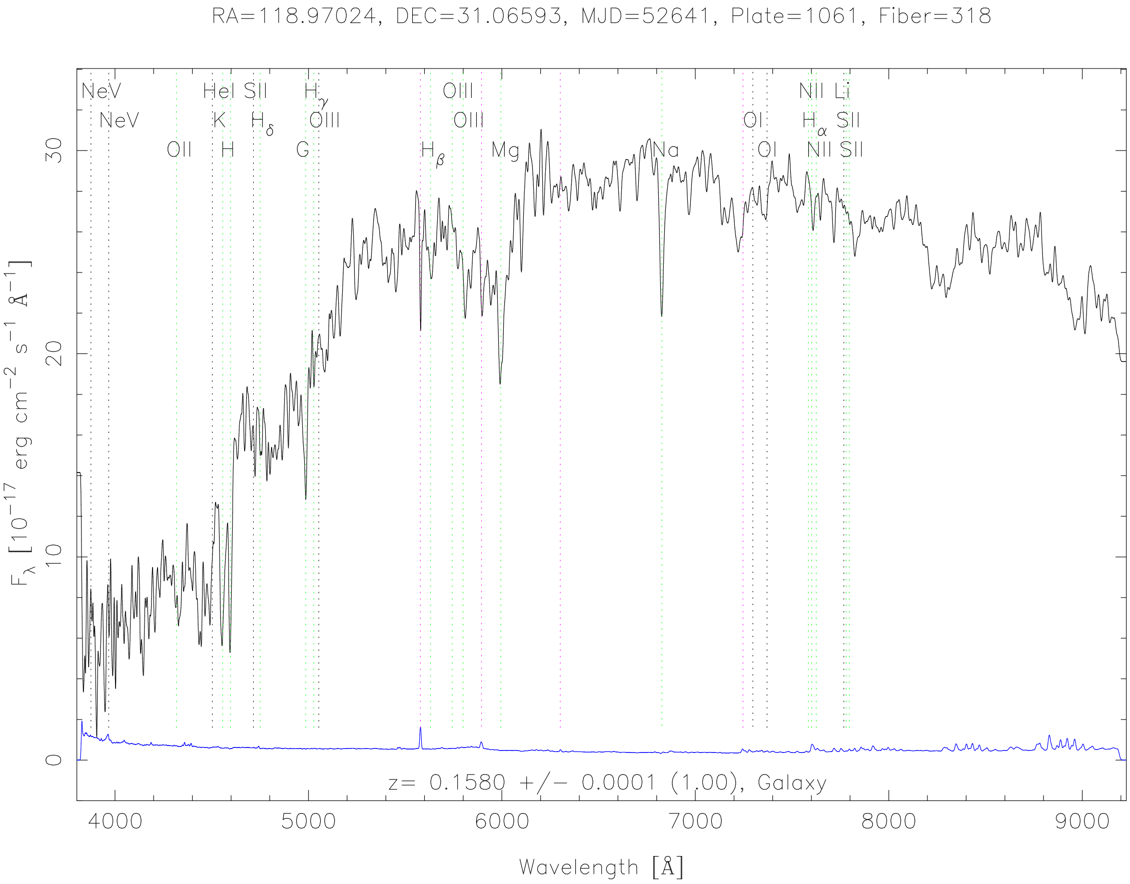

Fig. 17.— Spectrum for a typical elliptical galaxy as seen in the SDSS survey. The sharp step near 5400 Å allows for a good redshift measurement using color filters.

and calibration. Likewise, several large and ongoing ground-based galaxy redshift surveys (VIRMOS, DEEP) will also provide spectroscopic redshift samples that can help calibrate and verify photometric redshifts for the SNAP Wide Area Survey galaxy sample.

Finally, note that the development of reliable photometric redshift techniques is already an active area of research for several Fermilab SNAP group scientists who are involved in the SDSS. In particular we have extensive experience in the calibration of photometric redshifts from large redshift surveys like the SDSS and CNOC2, as well as from deep photometric samples such as the Hubble Deep Field. It will thus be very natural for Fermilab to take an active role in developing photometric redshift techniques for SNAP.

9.2. Cluster Finding

The SNAP telescope will image each galaxy in the wide-angle survey through nine different color filters, while taking detailed spectra for only a tiny subset. Therefore, the cluster identification and redshift measurements will have to rely on position information, combined with color information from these filters. There are several candidate cluster finding algorithms that take advantage of the precision colors. In the SDSS we have explored mostly the Adaptive Matched Filter and MaxBCG (e.g., Kim 2002c; Bahcall et al. 2003).

The technique of maximizing cluster likelihood around Brightest Cluster Galaxies (MaxBCG) uses the elliptical galaxies found by the survey, and exploits the following properties of galaxies and clusters:

1. Elliptical galaxies have very regular spectra, as illustrated in Fig. 17. In particular, there is a large step in the spectral intensity for wavelengths longer than the Calcium H and K lines. The intensity in the color filter containing this step, relative to intensities in neighboring filters, provides a measurement of the redshift adequate for identifying common members of a cluster. Elliptical galaxies have a very wide distribution of intrinsic brightness.

2. Clusters typically contain one elliptical galaxy with intrinsic brightness above the range of normal elliptical galaxies. These are called "Brightest Cluster Galaxies" (BCG) and their intrinsic brightness falls in a relatively narrow range.

The MaxBCG algorithm proceeds by:

1. Identify BCG candidates, and use these as seeds for the cluster search.

2. Assume a value for the redshift, and thus a distance to the BCG.

3. Look within a circle of 1 h^{-1} Mpc of the BCG for other elliptical galaxies. The size of this circle, projected on the sky, depends on the assumed value of the redshift. Include elliptical galaxies within a redshift window, as illustrated in Fig. 18, into a candidate cluster.

4. Calculate a likelihood, based on how well the observed BCG fits the brightness and color for a BCG at the assumed redshift, plus the ln of the count of galaxies inside the color range dimmer than the BCG and brighter than $1/2L_\star$ at the assumed z.

5. Find the value of the redshift that maximizes this likelihood.

6. A final step handles mergers in cases of overlap between candidate clusters.

In the case of SNAP, this algorithm can be used with different filters up to very high redshift.

In SDSS data, this technique has been able to measure the redshift z with an r.m.s. uncertainty of 0.019 (see figure 19). It has also been successful at separating clusters with different z even when they overlap in the sky. Furthermore, the technique has been shown to be $\approx 95\%$ complete down to $N_{red} = 15$ with $\leq 5\%$ contamination. This has been determined in two ways. The traditional approach is to add artificial clusters to the data stream and recover them. We note that this depends heavily on the input clusters. The more powerful technique is to take a sufficiently detailed and large scale N-body simulation and to put galaxies onto the dark matter particals in a fashion that reproduces clustering, luminosity and color statistics. This has the great benefit of allowing one to measure the simulation just as one would the sky but with a truth table behind it. We expect this technique to gain in power over the next decade.

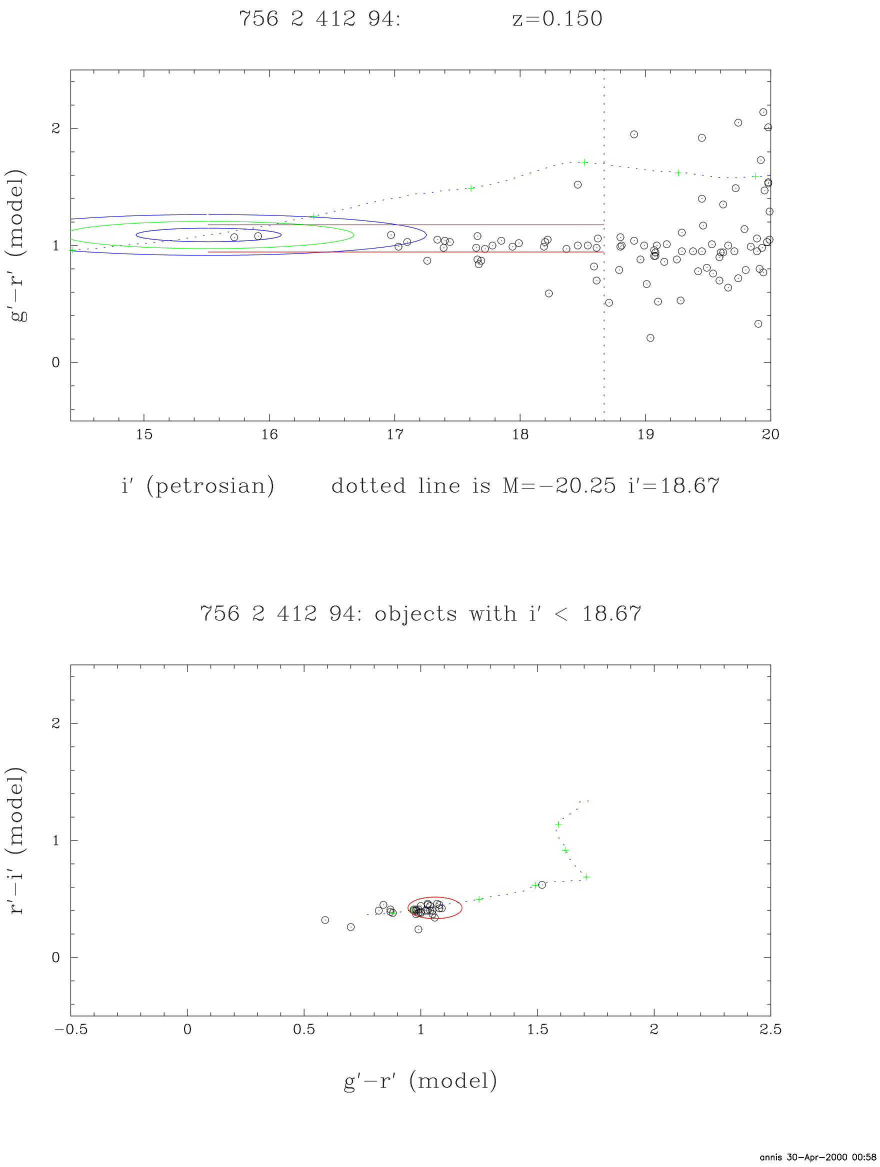

Fig. 18.— Illustration of the MaxBCG algorithm for a cluster in the SDSS survey. The vertical axis measures galaxy color, while the horizontal is the observed intensity in magnitudes. There is one data point for each galaxy within 1 h^{-1} Mpc of the BCG, calculated with an assumed value of the redshift. The horizontal dotted line shows the mean color-magnitude relation for BCGs, while the ellipse illustrates the range of deviation from the mean. The solid horizontal lines near the ellipse shows the color range for galaxies to be included in the calculation of N_{red}. The vertical dotted line is a luminosity cut-off, and depends on the assumed redshift. The lower plot shows the cuts in the color-color space: here one is just looking at points above the luminosity cut-off and inside the 1 h^{-1} Mpc radial cut and asking whether they lie within the colors expected for ellipticals at that redshift.

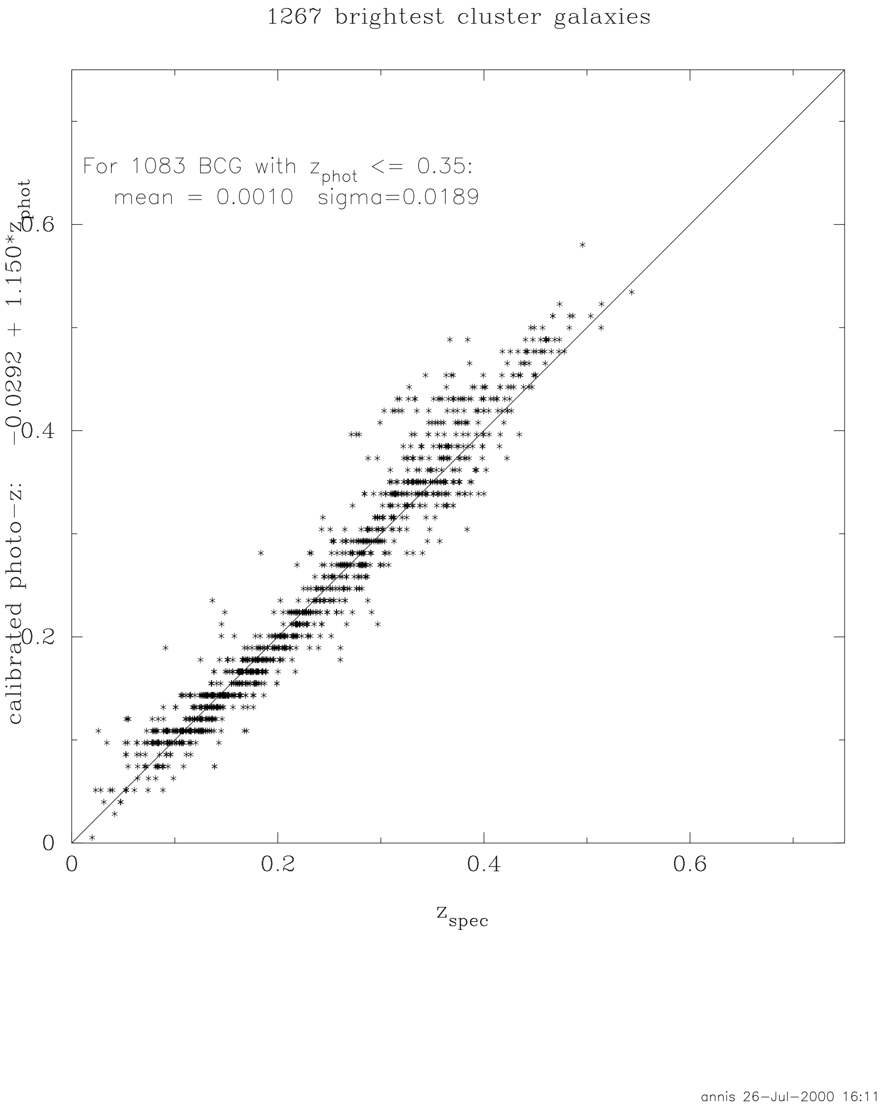

Fig. 19.— The photometric redshifts derived from the maxBcg cluster finding algorithm. The precision of this photo-z is sufficient that one does not need spectroscopic redshifts to pursue cosmology.

We have used the SNAP exposure calculator (Bernstein 2002) to estimate the capability of this algorithm for the redshifts accessible with SNAP. The results are shown in Fig. 20, which shows the signal-to-noise for galaxies at the lower luminosity cut-off of the MaxBCG algorithm. The S/N is very good for the longest wavelength filters, since these filters are wide and each galaxy gets two measurements in the highest bands. The S/N might be marginal for intermediate redshifts, which could translate into lower efficiency or higher confusion between clusters. However, we note that the filters simulated here are not yet the SNAP filter set. More work needs to be done to simulate the SNAP filter set, and establish the level of S/N that is adequate.

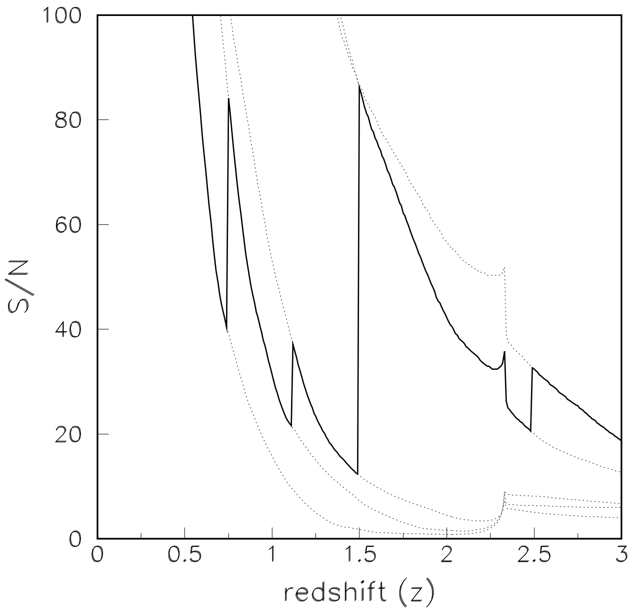

Fig. 20.— Signal To Noise in the r, i, z, J, and H filters (dotted curves, in order from left to right) for a galaxy at the luminosity cutoff for maxBCG at a variety of redshifts, for the case of Survey V in Table 2, and galaxies with FWHM = $0.3''$. These were calculated with the (Bernstein 2002) SNAP exposure calculator. The dark line shows the S/N for the band containing the 4000 Å break. As the 4000 Å break is redshifted, good S/N is required in succesively redder bandpasses, until at z = 2.4 it begins to enter the SNAP H band, and our method becomes impossible. It is worth noting that we can pursue our program until this point and that $z = 2.4$ is an impressively high z for cluster finding.

10. Summary

Supernovae provide the leading probe of dark energy, and the SNAP collaboration has made the case for SNAP being the leading dark energy experiment. Our emphasis is on strengthening SNAP's capability using two other probes: (i) weak lensing cosmic shear and (ii) the abundance of galaxy clusters as a function of mass and redshift. These methods are independent of the supernovae, subject to completely different systematic errors, and can thus provide important checks on the supernova results on w.

The eight survey options shown in Table 2 span a range of depths and survey areas—covering survey areas from 300 to 2000 square degrees, with the larger areas generally having shorter exposure times and consequently less depth. The philosophy was to design a wide field survey that could yield dark energy constraints of comparable or greater statistical precision than the SNAP supernovae, while still remaining in the depth regime that exploits the advantages of space. While we have not completed our exploration of this design space, our current results lead us to a 10 month/1000 sq-degree survey option: if that is what is needed to make these probes truly complementary in strength to the supernovae, it should be considered.

The trade off generally is to sacrifice depth in favor of area: the statistical errors on the cosmic shear power spectrum and on the cluster abundance both scale roughly as the inverse square root of the survey area. While increasing area implies less depth, the scaling of the errors with survey limiting depth is less strong.

For cluster counting, it appears that a 1000 sq-degree survey would provide a constraint on w of 0.05, comparable to the supernovae constraint. The data includes means to self-calibrate by using the weak lensing signal of stacked clusters even at the lowest masses and out to $z = 2.4$.

If we discount weak lensing information on the smallest scales because of theoretical uncertainties, and restrict ourself to linear scales where the shape-noise is small compared to the sample variance one is lead again to increase the area for greater statistical accuracy. Robust constraints on w of 0.05 result from a 1000 sq-degree survey.

SNAP as a wide-field imaging survey telescope would also be an unprecedentedly powerful tool for studying populations galaxies and quasars at high redshifts and faint magnitudes, as well as for constraining models for the formation and evolution of these objects. Fermilab SNAP group is specifically interested in the clustering properties of galaxies and and dark matter and the redshift evolution of galaxy populations.

Our studies indicate that increasing the sky coverage of the SNAP wide area survey can yield improvements in its Dark Energy reach. This may entail a need for larger data rate and overall data volume than currently envisioned for the mission. We describe a program of hardware related research being undertaken at Fermilab, aimed in part at achieving the wide area survey. This includes focal plane electronics, data compression, on-board storage, and data transmission. Along with the radiation shield, these are areas in which Fermilab expects to play a major role in the project.

The wide area survey also has special software requirements in addition to those for the supernova survey. Building on the expertise developed through experience in the Sloan Digital Sky Survey (SDSS), this is also an area where Fermilab plans to take on a leadership role, developing a pipeline for processing, co-adding, and analyzing the imaging data and technologies for a data factory and distribution.

The Fermilab group is driven by the scientific goal of uncovering the nature of the Dark Energy. The means to do so include the cluster counting and weak lensing methods as well as the supernovae methods. We are interested in all the methods, but are particularly interested in the prospects for the SNAP wide area survey. In addition to the technical hardware and software expertise we will bring to SNAP, Fermilab has the human talent and experience in place to play a major scientific leadership role in the wide area survey, regardless of its sky coverage.

REFERENCES

Abraham, R.G., et al. 1996, ApJS, 107, 1

Bacon, D.J, ,Refregier, A.R.,& Ellis, R.S. 2000, MNRAS, 318, 625

Bahcall, N. et al. 2003 ApJ, 585, 182

Bennett C.L. et al. 2003 astro-ph/0302207

Bershady, M.A., Jangren, A., & Conselice, C.J., 2000, AJ, 119, 2645

Bernstein, G. 2002, PASP, 114, 98

Blanton, M.R., et al. 2003, ApJ, in press (astro-ph/0210215)

Borgani, S., Rosati, P., Tozzi, P., Stanford, S. A., Eisenhardt, P. R., Lidman, C., Holden, B., Della Ceca, R., Norman, C., Squires, G., 2001, ApJ, 561, 13

Bower, R. G., Lucey, J. R., and Ellis, R. S. 1991, MNRAS, 254, 601

Carroll, S.M. 2001, Living Reviews in Relativity, 4, 1 (astro-ph/0004075)

Connolly, A.J., et al. 1995, AJ, 110, 2655

Cooray, A., and Sheth, R. 2002, Phys. Rep. 372, 1

Csabai, I., et al. 2003, AJ, 125, 580

Deustua, S. E., Caldwell, R., Garnavich, P., Hui, L., Refregier, A. 2001 Snowmass review, astro-ph 0207293

Ellis, R.S., et al. 1996, MNRAS, 280, 235

Frieman, J., Hill, C., Stebbins, A., and Waga, I. 1995, Phys. Rev. Lett. 75, 2077

Fry, J. N. 1994, Phys. Rev. Lett. 73, 215

Fry, J. N. & Gaztanaga, E. 1993, ApJ, 413, 447

Garnavich, P. M. et al. 1998, ApJ, 493, 53

Jarvis, M., Bernstein, G., et al. 2002, ApJ, in press (astro-ph/0210604)

Haiman, Z., Mohr, J. J., and Holder, G. P. 2001, ApJ, 553, 545

Huterer, D. & Turner, M. 2001, PRD, D64, 123527.

Huterer, D. 2002, PRD, D65, 063001.

Kim, R. S. J., et al. 2002, AJ, 123, 20

Kim, A. 2002, available at http://snap.lbl.gov/review/Final/SC1/Kim_SC1_final.ppt

Kim, A., Akerlof, C., et al. 2002, LBNL 51151, astro-ph/0210077.

Jenkins, A. et al. 2001, MNRAS, 321, 372

Lanzetta, K.M., Yahil, A., & Fernandez-Soto 1996, Nature, 381, 759

Levine, E. S., Schulz, A. E., and White, M. 2002, ApJ, 577, 569

Lilly, S.J., et al. 1995, ApJ, 455, 108

Lin, H., et al. 1999, ApJ, 518, 533

Massey, R., et al. 2003a, MNRAS, submitted (astro-ph/0301449)

Massey, R., et al. 2003b, ApJ, submitted (astro-ph/0304418)

Nordberg, P., et al. 2002, MNRAS, 336, 907

Peebles, P. J. E. 1980, Large Scale Structure of the Universe, Princeton University Press

Peebles, P. J. E. and Ratra, B. 2003, Rev. Mod. Phys. 75, 599 (astro-ph/0207347)

Perlmutter, S. et al. 1999, ApJ, 517, 565

Perlmutter, S. 2002a, available at http://snap.lbl.gov/review/Final/Plenary/Saul_Plenary_final_display_1.pdf

Perlmutter, S. 2002b, available at http://snap.lbl.gov/review/Final/SC1/Perlmutter_SC1_final2.ppt

Porciani, C., Giavalisco, M. 2002, ApJ, 565, 24

Press, W. H., and Schechter, P. 1974, ApJ, 187, 425

Riess, A. G. et al. 1998, AJ, 116, 1009

Refregier, A. 2003, MNRAS, 338, 35

Refregier, A., Massey, R., et al. 2003, ApJ, submitted (astro-ph/0304419).

Rhodes, J., Refregier, A., et al. 2003, ApJ, submitted (astro-ph/0304417).

Sawicki, M.J., Lin, H., & Yee, H.K.C 1997, AJ, 113, 1

Schade, D., et al. 1999, ApJ, 525, 31

Schmidt, B. P. et al., 1998, ApJ, 507, 46S

Sheldon, E. S. et al., 2001, ApJ, 554, 881

Scoccimarro, R., Feldman, H. A., Fry, J., Frieman, J. A. 2001, ApJ, 546, 652

Shapley, A.E., et al. 2001, ApJ, 562, 95

Simard, L., et al. 2002,

Spergel, D.N, et al. 2003, astro-ph/0302209

Steidel, C.C., et al. 1999, ApJ, 519, 1

Steidel, C. C., Giavalisco, M., Dickinson, M., Adelberger, K. L. 1996, AJ, 112, 352

Vanzella, E., et al. 2002, A&A, 396, 847

Williams, , et al. 1996, AJ, 112, 1335

Wilson, G., Kaiser, N., & Luppino, G.A. 2001, ApJ, 556, 601

Wittman, D.M., Tyson, J.A., Kirkman, D., Dell'Antonio, I., & Bernstein, G. 2000, Nature, 405, 143

van Dokkum, P.G., et al. 2003, ApJL, in press (astro-ph/0303166)

Van Waerbeke, L., Mellier, Y. et al. 2000, A&A, 358, 30

Van Waerbeke, L., Mellier, Y. et al. 2001, A&A, 374, 757

Wang, L., and Steinhardt, P. J. 1999, ApJ, 508, 483

This preprint was prepared with the AAS LaTeX macros v5.0.